

# NASA TECHNICAL MEMORANDUM

NASA TM X-64684

## FUNDAMENTAL CONCEPTS OF STRUCTURAL LOADING AND LOAD RELIEF TECHNIQUES FOR THE SPACE SHUTTLE

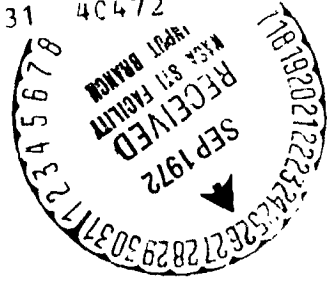
By R. S. Ryan, D. K. Mowery, and S. W. Winder  
Aero-Astroynamics Laboratory

August 18, 1972

(NASA-TM-X-64684) FUNDAMENTAL CONCEPTS OF  
STRUCTURAL LOADING AND LOAD RELIEF  
TECHNIQUES FOR THE SPACE SHUTTLE R.S.  
Ryan, et al (NASA) 18 Aug. 1972 76 p CSCL  
22B GJ/31

N72-31831

Unclass  
40472



**NASA**

*George C. Marshall Space Flight Center  
Marshall Space Flight Center, Alabama*

## TABLE OF CONTENTS

	Page
I. INTRODUCTION . . . . .	1
II. LOADING FACTORS (WHAT CAUSES VEHICLE LOADS) . . . . .	3
A. Aerodynamic Load Factors . . . . .	3
B. Thrust . . . . .	12
C. Acceleration . . . . .	13
D. System Moments . . . . .	14
III. LOAD REDUCING FACTORS (AUTOMATIC CONTROL) . . . . .	18
Wind Biasing . . . . .	19
IV. LOADS REDUCTION THROUGH ACTIVE CONTROL . . . . .	30
A. Rigid Body Dynamics . . . . .	30
B. Elastic Body (Modal Suppression) . . . . .	51
V. SYSTEM ANALYSIS AND CONCLUSIONS . . . . .	60
A. Performance Criteria . . . . .	64
B. Load Relief and Modal Suppression . . . . .	65
REFERENCES . . . . .	66

PRECEDING PAGE BLANK NOT FILMED

## LIST OF ILLUSTRATIONS

Figure	Title	Page
1.	Space Shuttle vehicle . . . . .	2
2.	Space Shuttle flight path . . . . .	2
3.	Aerodynamic force loading . . . . .	4
4.	Bending moment due to aerodynamics . . . . .	4
5.	Rigid body coordinates . . . . .	5
6.	Reference wind penetration . . . . .	7
7.	Aeroelastic effects . . . . .	9
8.	Beam analogy . . . . .	9
9.	Moment distribution . . . . .	10
10.	Deflection curve . . . . .	10
11.	Moment and force interchange . . . . .	10
12.	Bending moment . . . . .	10
13.	Deflection curve . . . . .	11
14.	Unsymmetrical mounting of orbiter and booster . . . . .	11
15.	$M'_\alpha$ and $M'_\delta$ versus vehicle station . . . . .	15
16.	Normal flow distribution for Saturn V . . . . .	16
17.	Normal force distribution for Saturn V derivative . . . . .	17
18.	Total moment factor . . . . .	18

## LIST OF ILLUSTRATIONS (Continued)

Figure	Title	Page
19.	Wind mean prediction and biasing . . . . .	20
20.	Wind biasing schemes . . . . .	26
21.	Skylab wind limits — 12 km altitude . . . . .	27
22.	Pitch and yaw bending moment versus vehicle roll attitude . . . . .	28
23.	Pitch and yaw bending moment versus wind azimuth . . . . .	29
24.	Attitude and velocity dispersions . . . . .	29
25.	Saturn V control frequency — drift root relationships . . . . .	32
26.	Shuttle control frequency — drift root relationships . . . . .	33
27.	Saturn V drift root versus angle-of-attack gain, $b_0$ . . . . .	37
28.	Shuttle drift root versus angle-of-attack gain, $b_0$ . . . . .	37
29.	S-IC Orbiter drift root versus angle-of attack gain, $b_0$ . . . . .	38
30.	Saturn V dynamic term coefficients — ramp wind . . . . .	39
31.	S-IC Orbiter dynamic term coefficients — ramp wind . . . . .	40
32.	Shuttle dynamic term coefficients — ramp wind . . . . .	40
33.	Shuttle dynamic term coefficients — ramp wind . . . . .	41
34.	Saturn V — step wind . . . . .	41
35.	S-IC = Orbiter, $c_1 = -1.87$ step wind . . . . .	42
36.	Shuttle — step wind . . . . .	43

## LIST OF ILLUSTRATIONS (Concluded)

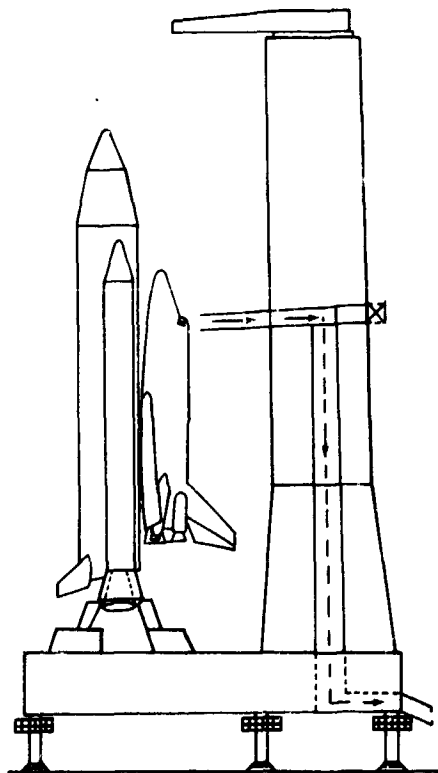
Figure	Title	Page
37.	Saturn V quasi-steady term coefficients — ramp wind . . . . .	44
38.	S-IC Orbiter quasi-steady term coefficients — ramp wind . . . . .	45
39.	Shuttle quasi-steady term coefficients — ramp wind . . . .	46
40.	Shuttle quasi-steady term coefficients -- ramp wind . . . .	47
41.	Saturn V — step wind . . . . .	48
42.	S-IC Orbiter, $c_1 = -1.87$ step wind . . . . .	49
43.	Shuttle — step wind . . . . .	49
44.	Shuttle dynamic response . . . . .	50
45.	Ratio influence of bending moment due to bending dynamics to total bending moment . . . . .	53
46.	Modal suppression . . . . .	57

## FUNDAMENTAL CONCEPTS OF STRUCTURAL LOADING AND LOAD RELIEF TECHNIQUES FOR THE SPACE SHUTTLE

### I. INTRODUCTION

Many studies have been made and numerous papers and reports written on the techniques of load relief. One can, therefore, justifiably raise the question: "Why add one more to the mass?" A survey of the many volumes shows that only one aspect of the problem has been treated at a time. Also, most of the published works deal only with aerodynamically unstable space vehicles or with aircraft gust loading. With the advent of the Space Shuttle vehicle concept, all of these characteristics are included (Figs. 1 and 2), and, therefore, a compilation of a treatment of the total problem is needed. The dynamics and control engineer must be concerned with loads resulting from attitude path control, as well as elastic body loading. This compounding of the problem makes it necessary to consider both the reduction of loads resulting from path control and from elastic mode suppression, the first designated "load relief" and the latter "modal suppression." Additionally, the vehicle can be highly aerodynamically unstable with large aerodynamic lift forces, or highly aerodynamically stable with even higher lift forces. The aerospace engineer is not accustomed to dealing with the large terminal path errors associated with large lift.

In order to properly assess load relief characteristics of a launch vehicle's control system, the engineer is concerned then with four major areas: (1) dynamic models for structure, liquid propellant, aerodynamic forces, control system, environment (atmospheric disturbances), and the overall combined system; (2) analysis techniques for frequency response, time response, and stability analysis, along with appropriate techniques for statistical description or interpretation of results; (3) criteria for evaluation of results, such as handling qualities, flutter boundaries, response goals, performance, constraints on control system, stability goals, design goals (probability of launch in worst wind month, etc.); and (4) control logic for alleviation or suppression of excessive loads. This paper covers loading factors, load reducing factors, trade factors, some typical results, and the further technology development that is needed.



- 156-IN. SOLID BOOSTER - PARALLEL-BURN EXTERNAL TANK ORBITER
- REUSABLE ORBITER, RECOVERABLE SOLIDS, THROW AWAY HO TANK
- VERTICAL TAKEOFF/HORIZONTAL LANDING
- LARGE CARGO CAPABILITY
- SHIRT-SLEEVE ENVIRONMENT FOR CREW AND PASSENGERS
- ACCEPTABLE G LOADS FOR NON-ASTRONAUTS
- 7 DAYS SELF-SUSTAINING
- APPROACH TO AIRLINE-TYPE OPERATIONS
- LOW COST

Figure 1. Space Shuttle vehicle.

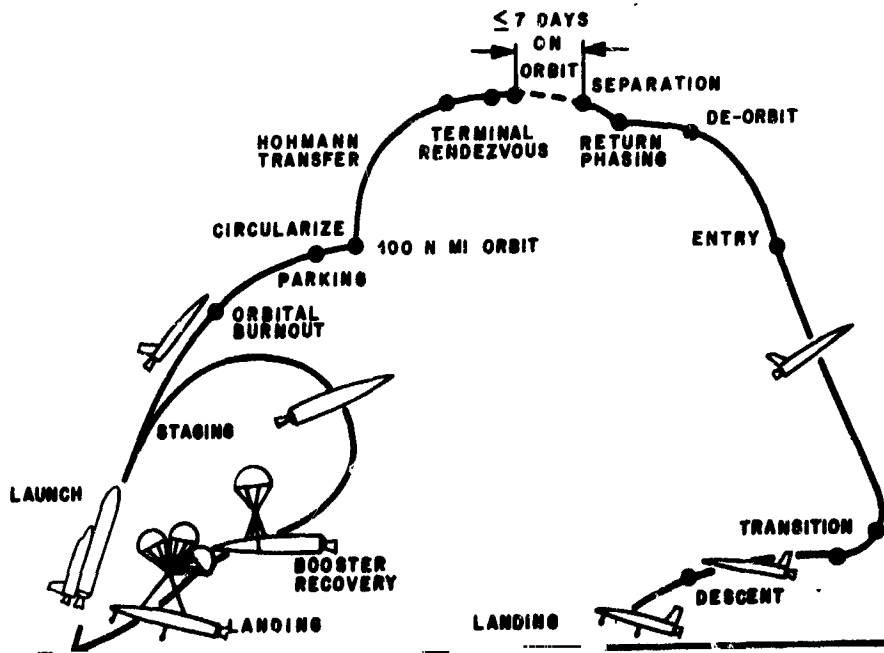


Figure 2. Space Shuttle flight path.

## II. LOADING FACTORS (WHAT CAUSES VEHICLE LOADS)

As a vehicle seeks a prescribed path in space, external disturbances [atmospheric forces, path control forces, propulsion forces, mass asymmetries, and component misalignments (thrust, center of gravity, etc.)] produce structural loads. The calculation of these complete loading histories for unsymmetrical, lifting surface vehicles is a formidable task, and must be accurately performed. Many of these load-producing factors cannot be easily reduced through control system logic. For simplicity and better insight, we will concern ourselves with only the normal loading factors (pitch or yaw plane), since these are the main effects the control system can alter.

Also, only a planar case will be used for simplicity, although extension to a 3-D case is obvious. Any attempt to reduce vehicle loading to parts is superficial, and any attempt to really understand vehicle loading must include the elastic 3-D vehicle and a 6-D trajectory using both aerodynamic surfaces and gimbal engines for control. However, much insight can be gained through the planar approach.

### A. Aerodynamic Load Factors

1. Basic Influence. As a space vehicle flies through the atmosphere, any deviation of the outer geometric surface from a zero angle of attack (relative airflow) creates aerodynamic forces which cause structural loading. Because of the different incidence angles relative to the body centerline, various components, such as wings, fins, etc., do not necessarily have simultaneously the same angle of attack. Therefore, the vehicle experiences an almost continuous loading even in a trim condition.

Figure 3 shows a typical aerodynamic load distribution for a space vehicle at some angle of attack,  $\alpha$ . The structural loading resulting from these aerodynamic forces can best be expressed as a bending moment, which is easily calculated as the sum of the products of the individual forces and their distance to the vehicle station of interest. Calculations of the bending moment envelope because of aerodynamic loading as a function of vehicle stations results in the characteristics per unit angle of attack shown in Figure 4.



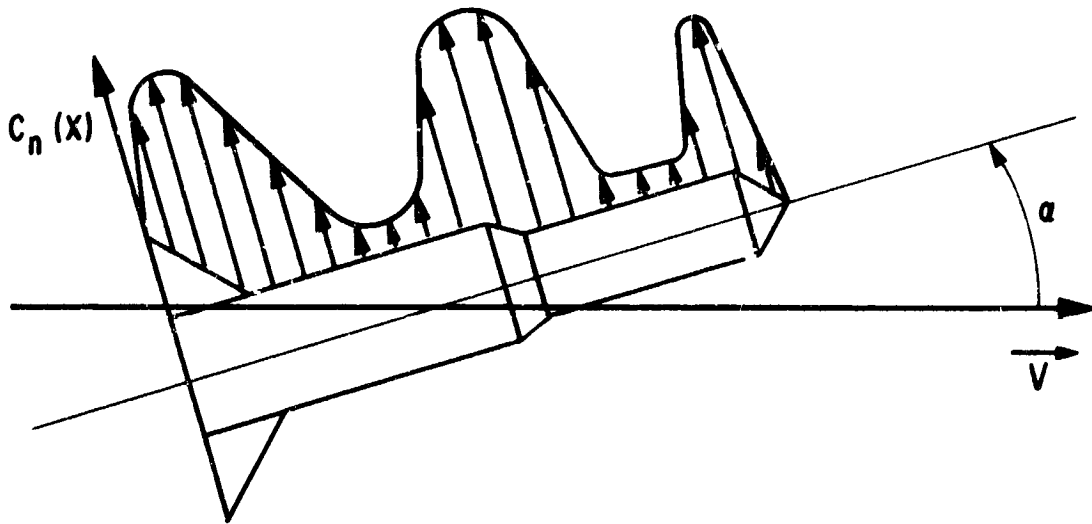


Figure 3. Aerodynamic force loading.

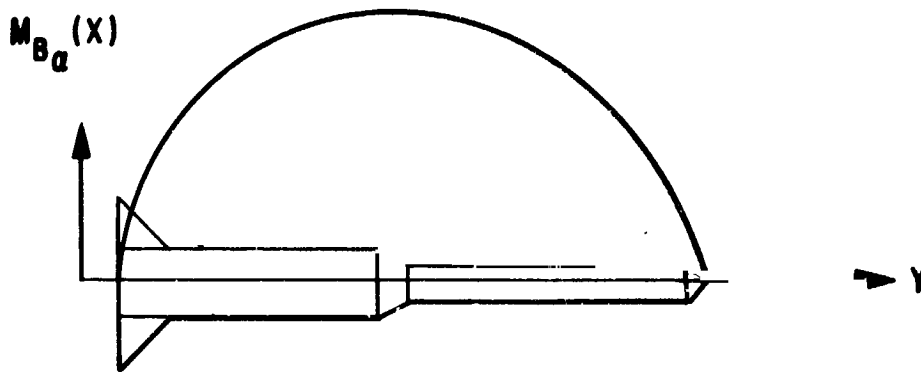


Figure 4. Bending moment due to aerodynamics.

This simple approach does not hold for many Space Shuttle concepts, such as a piggyback orbiter/booster mounting which assumes that the separation mechanism carries both the lateral and longitudinal loads. This complication is recognized, but for simplicity, is not included in our analysis. However, the omission should not detract from the basic conclusions. In order to calculate the bending moment resulting from aerodynamics, the angle of attack must be defined. Figure 5 illustrates the sign convention and vehicle states necessary for this definition, which includes vehicle attitude, vehicle velocity, wind velocity, and engine deflection angle.

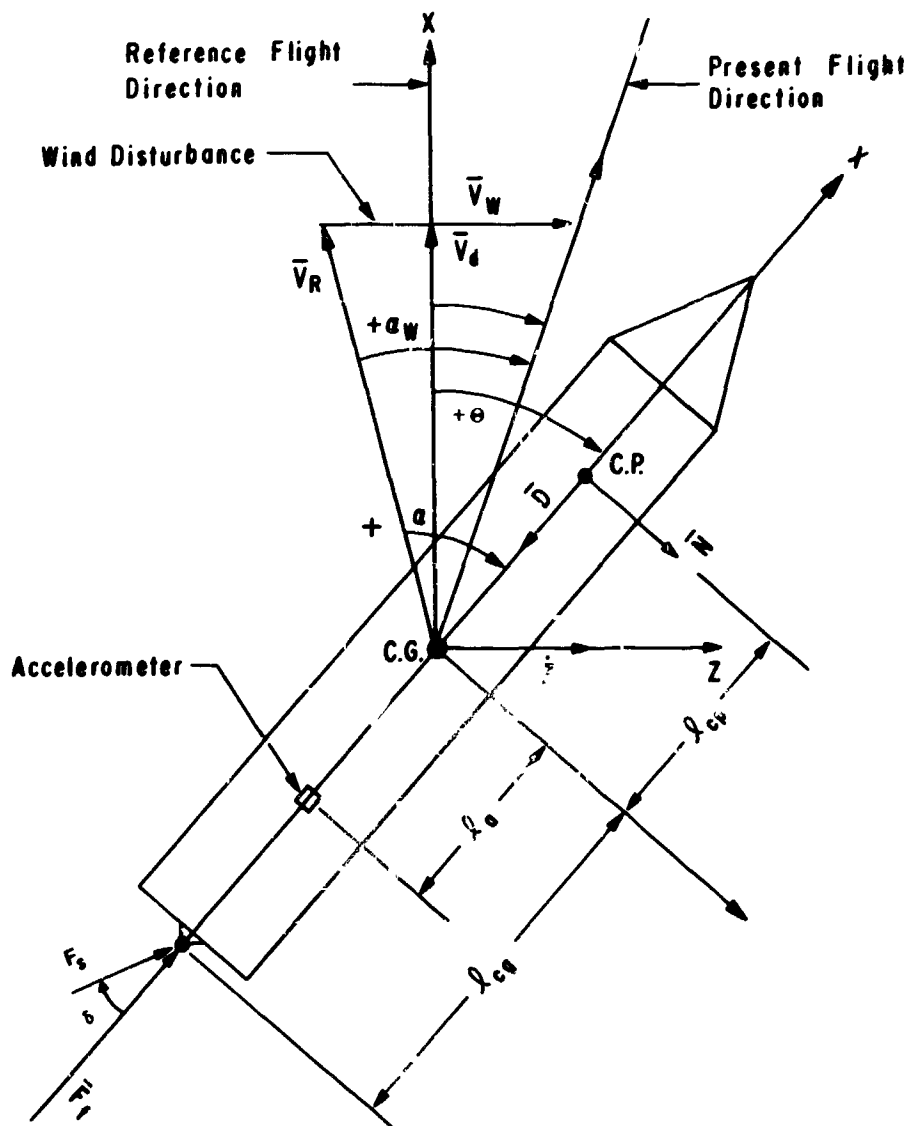


Figure 5. Rigid body coordinates.

Using these states, the angle of attack becomes

$$\alpha'(x) = \overbrace{\theta - \frac{1}{v} \left[ \dot{z} - (x_{cg} - x) \dot{\theta} \right] + \frac{V_W}{v}}^{\alpha_{\text{rigid}}} + \overbrace{\frac{1}{v} \sum_{\mu=1}^n \eta_{\mu} Y_{\mu}(x) - \sum_{\mu=1}^n \eta_{\mu} Y_{\mu}'(x)}^{\alpha_{\text{elastic}}} = \alpha_{\text{rigid}} + \alpha_{\text{elastic}} \quad (1)$$

The bending moment due to aerodynamics is

$$M_{B_{aero}} = \frac{qs}{D_0} \int_{X_T}^{X_k} C_Z(\alpha, x, M) (X_k - x) dx, \quad (2)$$

where  $q$  is dynamic pressure,  $s$  the base area,  $D_0$  the reference diameter,  $X_T$  the vehicle end station, and  $X_k$  the station where the bending moment is desired.

If the aerodynamics are linear and no bias lift forces exist (canted aerodynamic surfaces), the conventional form for  $C_Z(\alpha, x, M)$  is

$$C_Z(\alpha, x, M) = C_{Z\alpha}(x, M) \alpha(x) \quad (3)$$

This equation simplifies calculation and provides a means of expression for the bending moment. Where the aerodynamics are nonlinear and contain bias forces, equation (2) is quite cumbersome and is thus usually reduced to a summation of basic force tables which are a function of Mach number, local angle of attack, and dynamic pressure. When bias aerodynamic forces exist, but the forces about the bias are linear with angle of attack, equation (3) becomes

$$C_Z(\alpha, x, M) = C_Z(x, M) + C'_{Z\alpha}(x, M) \alpha(x), \quad (4)$$

which is, again, easy to solve. Further complications are introduced by the lifting surfaces because both spanwise and chordwise distributions exist, and load transfer to the fuselage makes the loads highly dependent on the configuration.

**2. Additional Considerations.** The effect of aerodynamics upon the load factor has been fairly straightforward up to this point. However, two additional effects occur which can have major impacts and must be considered: gust penetration and static aeroelasticity. Gust penetration effects are caused by the wind-induced angle of attack having frequency components. This means that the angle of attack along the vehicle changes due to this traveling wave effect of the wind gust (Fig. 6). Gust penetration becomes influential when the changing angles of attack (aerodynamic forces) along

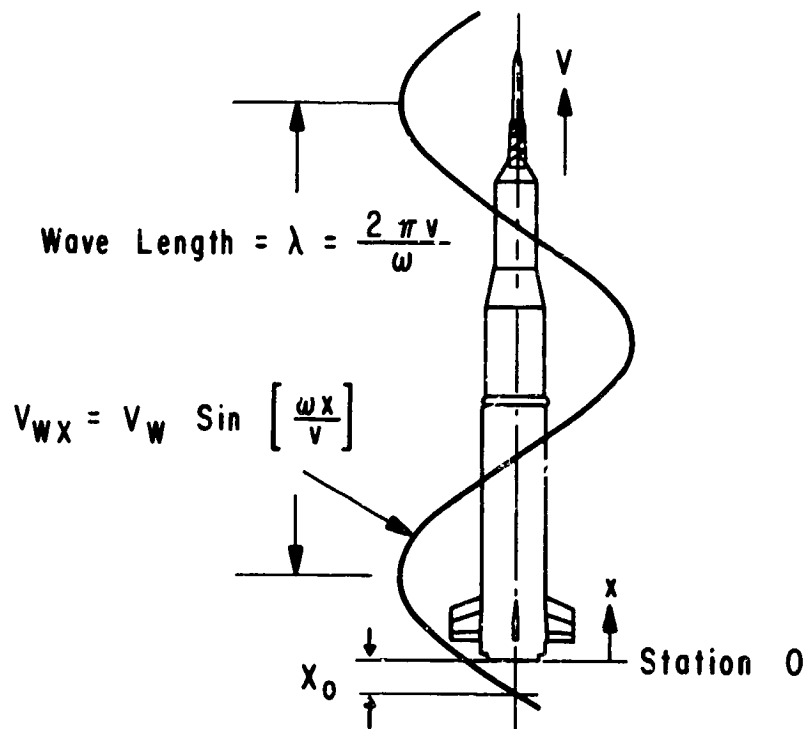


Figure 6. Reference wind penetration.

the vehicle are phased such that they add energy to the system. This effect can become severe for certain elastic mode shapes and gust frequencies. Also, the effect can be pronounced on aerodynamic control surfaces if the gust wave is out of phase at certain frequencies. In this case, the surfaces either become less effective or they add energy to a mode which introduces negative damping. It is quite cumbersome to include this effect in equation (1) if a time solution to the describing equations is desired. In this case  $V_W$  becomes a function of the vehicle station as well as altitude. If we use the vehicle tail as the reference altitude and time point, then the wind velocity at any station becomes

$$V(h)_{\text{vehicle station}} = V_W(h_0 + x) \quad , \quad (5)$$

where  $h$  is the altitude defined from the trajectory and is therefore a function of the vehicle velocity or time. In general, this approach is not used because of its complexity. To avoid this complexity, a frozen time-point analysis is made in the frequency domain which allows  $V_{WX}$  to be expressed fairly simply as

$$V_{WX} = V_W \sin \frac{\omega X}{v} \quad , \quad (6)$$

and

$$\lambda = \frac{2\pi v}{\omega} \quad .$$

By using a spectrum of the wind turbulence and a generalized harmonic analysis response approach, the basic terms and effects can be determined [1, 2].

Aeroelasticity is a particularly important factor in determining the quasi-steady state flight loads of a vehicle because, in a flight environment, the vehicle's deflected shape (elastic body bending) produces changes in local angle of attack. These changes will induce an additional aerodynamic loading which causes further increases or decreases in local angles of attack. The resultant deflected shape is an equilibrium between local aerodynamic forces and vehicle stiffness [3, 4]. To account for this effect, the aerodynamic distribution must be altered, or corrected values added to the total load (bending moment). Both approaches have been found to be accurate for launch vehicles. The principal cause of the aeroelastic effects is illustrated in Figure 7. Shown in this figure is an aerodynamically unstable vehicle which has the aerodynamic center in front of the center of gravity and the control force behind the center of gravity. Balancing wind-induced rigid-body angle of attack with the control force bends the vehicle such that the aerodynamic angle of attack is increased forward of the cg and decreased aft of the cg, making the vehicle more unstable. The opposite is true for aerodynamically stable vehicles. This explanation is obviously oversimplified since it does not include the total effect of inertial and aerodynamic forces.

The more complex effect can be simply illustrated by using a vehicle with two point forces and two acceleration forces. This assumption is not a bad one for some Shuttle configurations (interim) where a large mass and a large aerodynamic surface are near the vehicle nose, and a large mass (booster lox) and a large force (engines) are near the rear of the vehicle. In trimmed flight, the inertia, control, and aerodynamic forces balance.

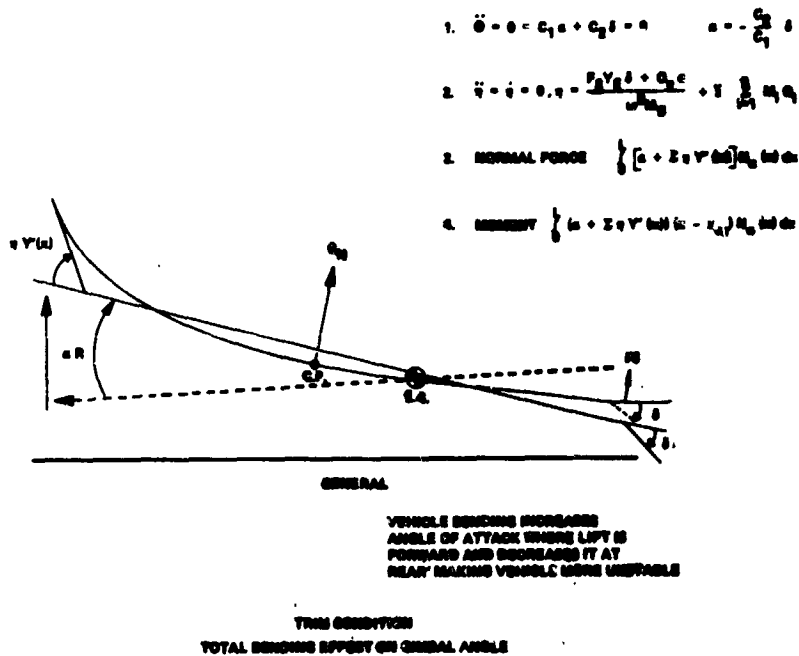


Figure 7. Aeroelastic effects.

Using this example, the bending moment equation becomes

$$EI(x) Y''''(x) = M(x) \quad (7)$$

The basic beam analogy is seen in Figure 8,

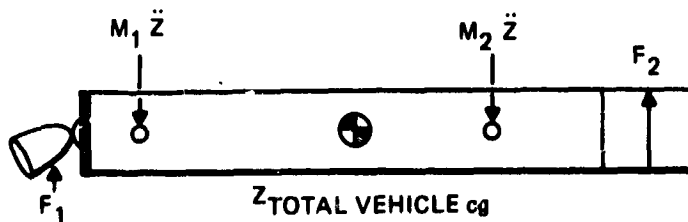


Figure 8. Beam analogy.

where  $F_1$  is the lateral control force,  $F_2$  is the induced trim aerodynamic force, and  $M_1 \ddot{z}$  and  $M_2 \ddot{z}$  are the inertial forces concentrated at the assumed cg's. The resulting moment distribution takes the shape seen in Figure 9.

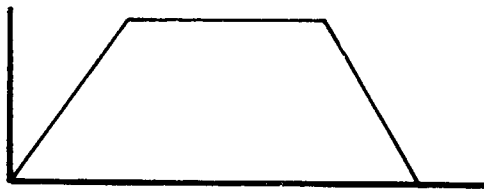


Figure 9. Moment distribution.

The deflection curve (Fig. 10), which increases the angle of attack of the vehicle nose, makes the vehicle more unstable since the aerodynamic forces are all assumed to act there.

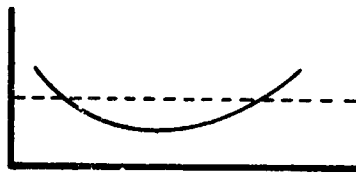


Figure 10. Deflection curve.

An interesting thing happens if locations of the forces  $M_2 \ddot{z}$  and  $F_2$  interchange. This can be seen in Figure 11.

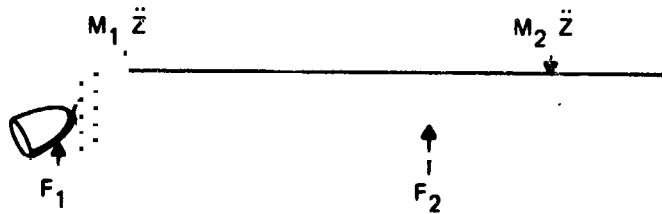


Figure 11. Moment and force interchange.

Here, the bending moment has the following general shape seen in Figure 12.

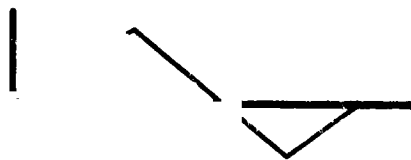


Figure 12. Bending moment.

The deflection curve (Fig. 13), which decreases the angle of attack at the location of the aerodynamic surfaces makes the vehicle more stable, just the opposite effect from what one would expect from our original oversimplified explanation.



Figure 13. Deflection curve.

For most Shuttle vehicles, an addition term must be added to include the unsymmetrical mounting of orbiter and booster. This term represents the moments which result from longitudinal acceleration forces and aerodynamic drag (Fig. 14) which, in turn, results in increased angle of attack of the vehicle nose.

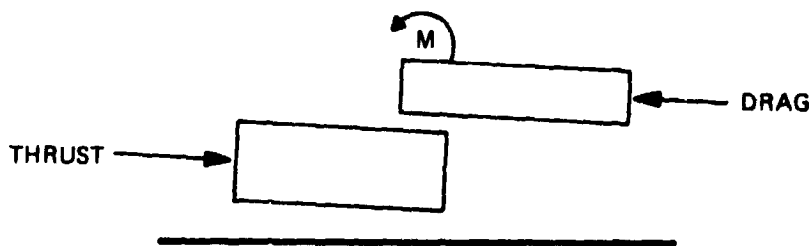


Figure 14. Unsymmetrical mounting of orbiter and booster.

To properly evaluate the Shuttle vehicle from the aeroelastic standpoint obviously would require a fairly complex analysis. However, a simple method for estimating the aeroelastic effect on stability is illustrated in Figure 7. Here, it is assumed that the vehicle is in a rigid-body trim condition and that no bending mode and rotational dynamics are involved ( $\ddot{\theta} = \dot{\theta} = \ddot{\eta} = \dot{\eta} = 0$ ). Thus, the static bending deflection ( $\eta$ ) for each mode can be calculated with the corresponding normal force and aerodynamic moment. This calculation, which has been shown to be fairly accurate, gives the approximate change in vehicle aerodynamic stability and permits a speedy prediction of loads and control system requirements. Also influential in these static aeroelastic lift growth effects is the downwash. As the vehicles become more complicated, i.e., more unsymmetrical with larger lifting surfaces, the difficulty of analysis of these effects increases by several orders of magnitude.



It should be pointed out here that gust penetration, lift growth, and downwash not only affect the bending moment directly, but they also indirectly affect the vehicle dynamics (to be discussed later). An additional word of caution: The factors that increase the complexity of analysis (unsymmetrical bodies, lifting surfaces) also increase the effects of gust penetration and static aeroelasticity. Therefore, these factors cannot be neglected as they have been in the analysis of the simple symmetrical space vehicles and missiles.

## B. Thrust

1. Rigid Body. The longitudinal thrust creates a normal load on the vehicle through swiveling of the engine for control. This swiveling introduces a moment at any station  $X_k$ . The bending moment equation due to thrust is

$$M_{\delta \text{ thrust}} = F_s X_k \sin \delta \quad , \quad (8)$$

and for small angles it is

$$M_{\delta \text{ thrust}} = F_s X_k \delta \quad . \quad (9)$$

If the vehicle center of gravity is offset laterally, the engines null the resulting moment by aligning with the thrust vector through the cg (in the absence of other torques). This offset causes the vehicle to fly cocked, thus introducing loads through the nominal terms present in equations (2) and (9).

2. Elastic Body. Two of the terms in the bending moment equation result from the vehicle being elastic. One is the moment due to the perpendicular forces and the other is the moment due to the parallel forces:

Perpendicular forces

$$M_{B \text{ thrust } (\perp)} = F_s X_k \sum_{\mu=1}^n \eta_{\mu} \left[ Y_{\mu}^{\circ} (X_k) - Y_{\mu}^{\circ} (X_s) \right] \quad , \quad (10)$$

and

Parallel forces

$$M_{B \text{ thrust } (\parallel)} = T \sum_{\mu=1}^n \eta_{\mu} \left[ Y_{\mu} (X_E) - Y_{\mu} (X_k) \right] \quad . \quad (11)$$

There is also an additional longitudinal coupling into the lateral plane caused by dynamic mass asymmetry coupling, which, because of its complexity, is not shown. A good example is the pogo -- longitudinal, lateral control coupling (called "hula pogo") which is of quite some concern for piggyback Shuttle vehicles. This problem will be the subject of a future paper.

### C. Acceleration

The lateral acceleration of any mass element in a vehicle creates a lateral force which results in an increased structural load (lateral bending moment). By summing up the product of these accelerations, the masses, and the distance to the station of concern, the bending moment effect is obtained.

1. Rigid Body. For a rigid vehicle in translation and rotation, the resulting acceleration of any station is

$$A(x)_{\text{rigid}} = \ddot{z} - (X_{\text{cg}} - x) \ddot{\theta} \quad , \quad (12)$$

and the corresponding bending moment is

$$M_{\text{B}_{\text{inertial rigid}}} = - \int_{X_{\text{T}}}^{X_{\text{k}}} m^{\circ}(x) (X_{\text{k}} - x) A(x)_{\text{rigid}} dx \quad . \quad (13)$$

2. Elastic. Vehicle vibrations also accelerate the individual mass elements that produce forces. These accelerations are as follows:

$$A(x)_{\text{elastic}} = \sum_{\mu=1}^n \ddot{\eta}_{\mu} Y_{\mu}(x) \quad , \quad (14)$$

and the resulting moment because of bending acceleration forces becomes

$$M_{\text{B}_{\text{elastic}}} = - \int_{X_{\text{T}}}^{X_{\text{k}}} m^{\circ}(x) (X_{\text{k}} - x) A(x)_{\text{elastic}} dx \quad . \quad (15)$$

## D. System Moments

When these various contributions are collected, we have the total system bending moments on the vehicle. The contribution to the vehicle normal structural loading has been presented. These bending moment equations (2, 8, 9, 10, 11, 15), as given, are a function of the angle of attack, engine deflection, and vehicle accelerations. Also, the fact that the vehicle accelerations are in turn a function of the angle of attack and engine deflection allows the expression of the bending moment in simpler terms, through substitution for the accelerations. These substitutions allow the loading (bending moment) to be expressed for the linear angle-of-attack case (including local angle-of-attack effects) as

$$\begin{aligned}
 M_B(x,t) = & M'_\alpha(x) \alpha_{\text{rigid}}(t) + M'_\delta(x) \delta(t) + M'_{\dot{\theta}}(x) \dot{\theta}'(t) \\
 & + \sum_{\mu=1}^n M'_{\dot{\eta}_\mu}(x) \dot{\eta}_\mu(t) + \sum_{\mu=1}^n M'_{\eta_\mu}(x) \eta_\mu(t) \\
 & + \sum_{\mu=1}^n M'_{\ddot{\eta}_\mu}(x) \ddot{\eta}_\mu(t) + \sum_{\mu=1}^n M'_{\ddot{\xi}_s}(x) \ddot{\xi}_s(t) + M_{B0}
 \end{aligned} \tag{16}$$

In the many cases where several terms have only minor effects, equation (16) can be reduced to

$$\begin{aligned}
 M_B(x,t) = & M'_\alpha(x) \alpha_{\text{rigid}}(t) + M'_\delta(x) \delta(t) + \sum_{\mu=1}^n M'_{\ddot{\eta}_\mu}(x) \ddot{\eta}_\mu(t) \\
 & + M_{B0}
 \end{aligned} \tag{17}$$

If the effects of nonlinear aerodynamics, gust penetration, static aeroelasticity, and bias aerodynamics are important, equations (1) through (17) become very complex even for the planar case.

To gain insight into some of the influences of various factors on the structural loading (bending moment), equation (17) was analyzed for a conventional Saturn-type vehicle. To see one of the effects of the aerodynamic forces, the vehicle aerodynamic characteristics were parameterized

by adding fins at the rear. For simplicity, it was assumed that no mass change occurred in obtaining the added lift. Figure 15 is a plot of the  $M'_\alpha$  and  $M'_\delta$  for these changing aerodynamic characteristics. Both the conventional aerodynamic unstable configuration and an induced stable configuration ( $C_1 < 0$  and  $C_1 > 0$ , respectively) are shown. Very little change occurs in  $M'_\delta$  as the aerodynamic characteristics are changed; however,  $M'_\alpha$  increases greatly with the added lift necessary to make the vehicle stable.

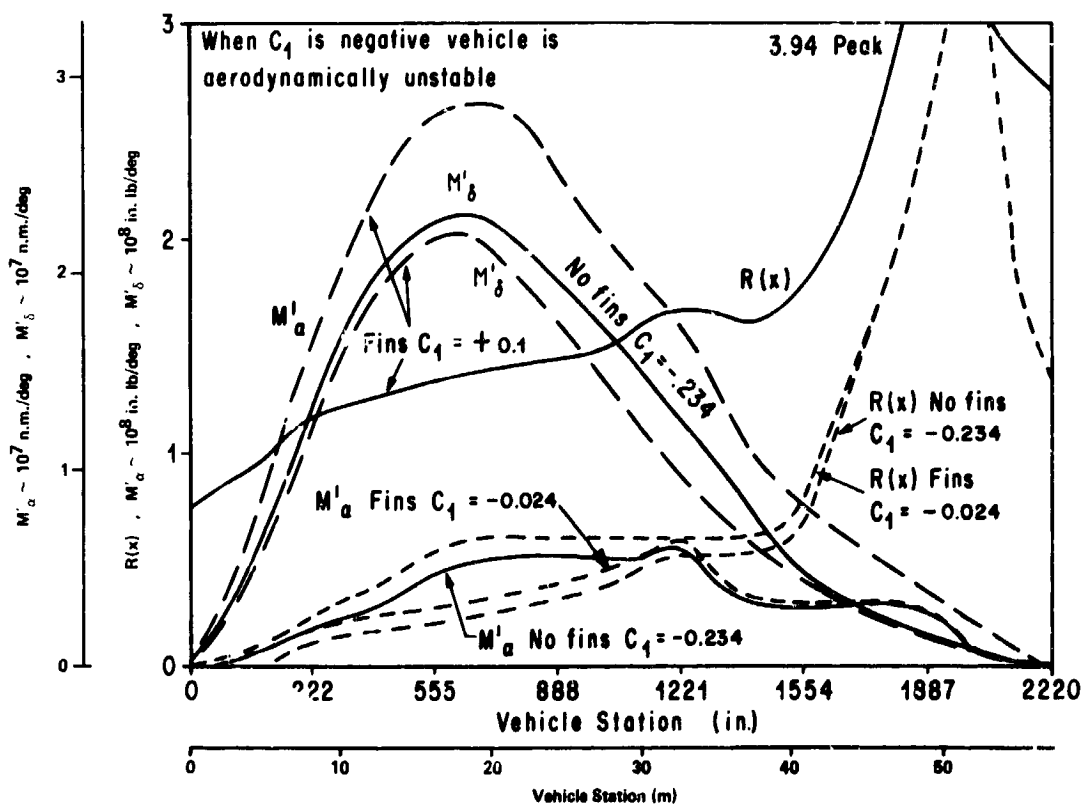


Figure 15.  $M'_\alpha$  and  $M'_\delta$  versus vehicle station.

Also, shown on Figure 16 is the ratio,  $R(x)$ , of  $M'_\alpha$  to  $M'_\delta$ , which clearly shows that, for vehicle stations where angle-of-attack effect is large, i. e., where  $R(x)$  is large, a control logic that reduces  $\alpha$  by increasing  $\delta$  can generally be used to reduce loads. If the converse is true, i. e.,  $R(x) < 1$ , very little can be done with this approach.

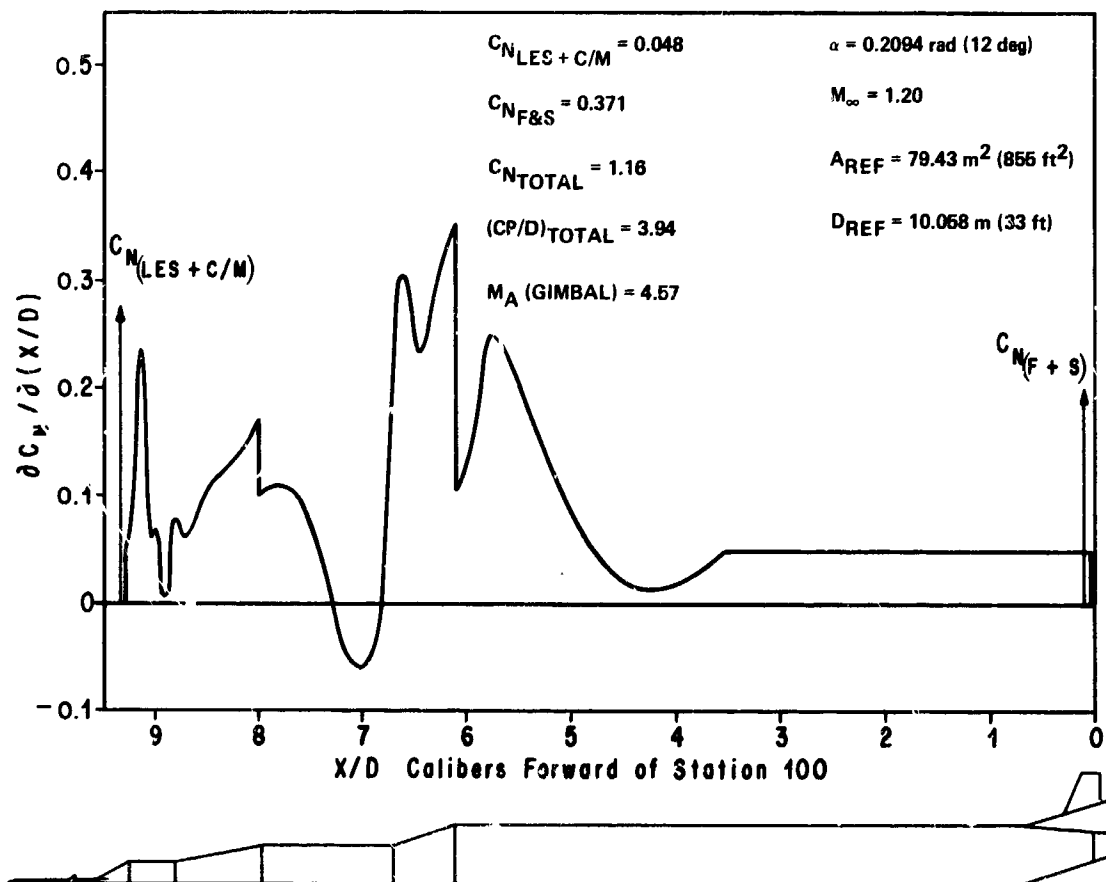


Figure 16. Normal flow distribution for Saturn V.

An additional effect of the aerodynamic distribution on the  $M_\alpha$  is shown on Figures 16 through 18. Figures 16 and 17 show the distributions, and Figure 18, the resulting  $M_\alpha$ 's normalized to the same value. As shown on Figures 17 and 18, the total aerodynamic moment about the gimbal is increased by only 30 percent between the Apollo and the INT-21 configurations. However, the total aerodynamic contribution to the  $\alpha$  part of the bending moment goes up by a factor of 2 to 3 on the front half of the vehicle. This increase in the aerodynamic contribution is due to the fact that the Apollo has a distribution that can be approximated by three point forces, while the INT-21 is approximated by two point forces. What happens is that the third point force near the middle of the vehicle acts to shorten the lever arm over which part of the total force acts, thus reducing the bending moment, although the total lift force acting on the vehicle increases by 10 percent and

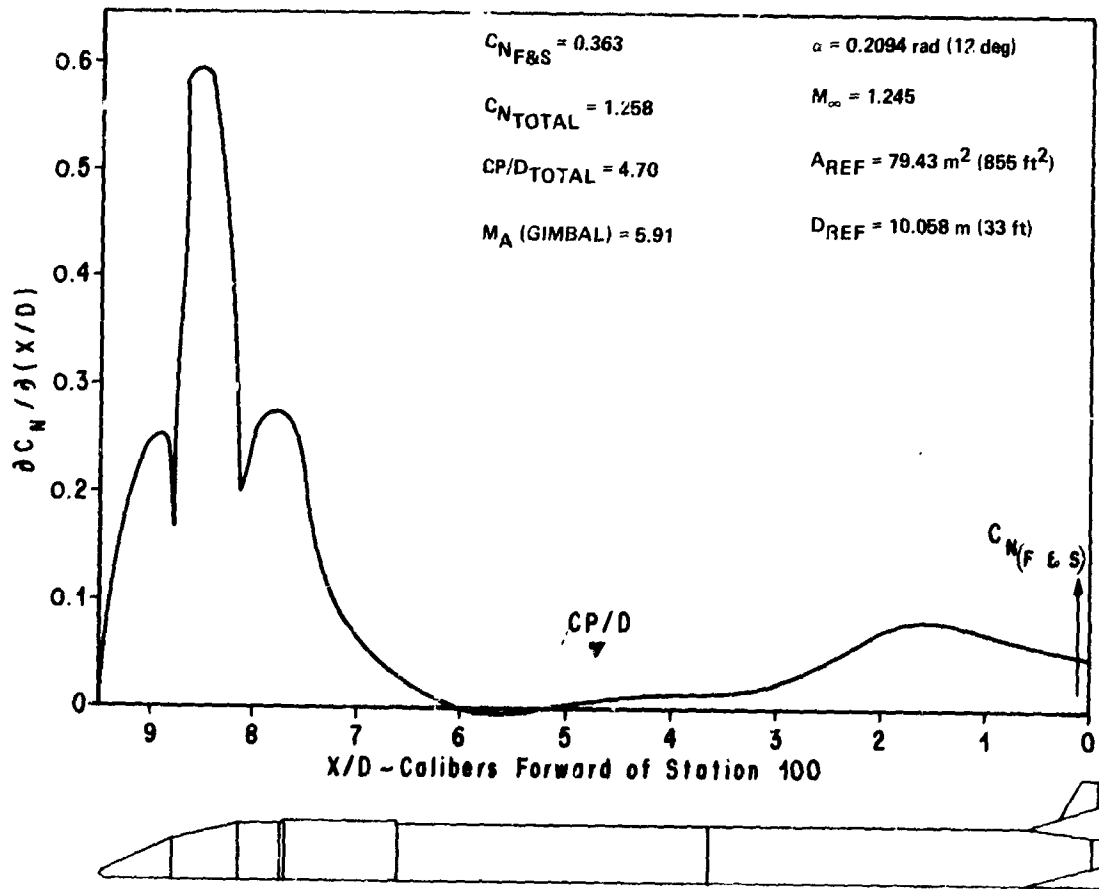


Figure 17. Normal force distribution for Saturn V derivative.

the restoring moment by 30 percent. This comparison clearly shows that load relief can be accomplished through aerodynamic shaping. There are many aspects of these aerodynamic shaping considerations which should be explored for the Shuttle.

Analysis of the load-producing factors makes several conclusions evident:

1. There is a direct correlation between the bending moment, aerodynamic, and mass distribution. It is not possible to ascertain analytically how they are correlated because of the complexity of the equations. Vehicle dynamics are also a strong function of the same aerodynamic and mass distributions.

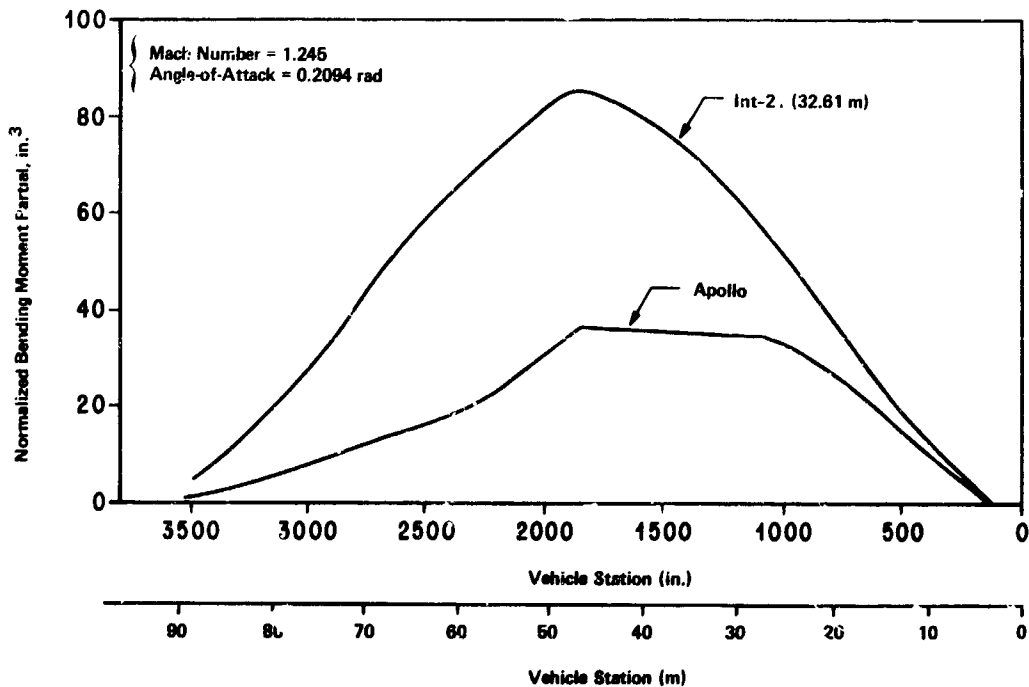


Figure 18. Total moment factor.

2. Static bending deflection, angle of attack, and bending dynamics should be kept as low as possible in order to reduce aeroelastic effects of gust penetration and static aeroelasticity.

3. Vehicle loads from engine deflection versus those from angle of attack are strongly dependent upon vehicle station with no two classes of vehicles being the same. This indicates that any load relief scheme becomes highly dependent upon vehicle station.

4. Vehicle loads can be reduced through configuration design (aerodynamic and mass distributions).

### III. LOAD REDUCING FACTORS (AUTOMATIC CONTROL)

In the previous section, basic load producing factors were presented and some conclusions drawn pertaining to their respective interaction. These loading factors, if not kept within certain bounds, can heavily penalize the vehicle payload through increased structural weight or reduced launch windows due to launch restrictions. If mission constraints dictate that neither the weight penalty nor launch restrictions can be allowed, then some

means of alleviating these load conditions must be found. The most promising approach is through some means of active control, whether it be adaptive or programmed gains. Also, it would be advantageous if it were optimal in terms of loads. However, this is usually not possible because of other constraints, such as terminal drift, attitude path dispersions, and performance constraints. Inflight winds are, of course, the major disturbance of nominal ascent flight and cause both control forces to be applied and angle of attack to build up. Load reduction then becomes intimately related to the vehicle response to winds. As implied by previous discussion, both a reduction in normal force because of control and a reduction in normal force because of angle of attack (most of which is induced by wind effects) can be used to reduce structural loading. However, simultaneous reduction of both the control force and angle of attack is not necessarily compatible, so that some knowledge of the structural capabilities of the vehicle is essential to achieve load reduction in the more critical places and to indicate which of the two forces can be reduced most profitably. Load reduction can then be accomplished in several ways, all of which must be understood and be available for specific situations. In general, load reduction techniques can be separated into two categories: passive and active. The passive approaches usually prohibit launch when winds are greater than a limiting value with prelaunch wind monitoring and wind biasing, both preflight (monthly mean) and inflight (previous days mean). Active schemes either feed back a measurement of the wind or some vehicle state, such as angle of attack, body-fixed acceleration, body-fixed velocity, and vehicle position. How these various approaches affect load reduction is a function of the vehicle flight mechanics and flight dynamic characteristics, as well as vehicle station. In many cases the effects are contradictory, and what helps in one situation hurts in another. This will be discussed in more detail later. For simplicity, the discussion of wind effects is separated into three parts: the deterministic wind (wind biasing), the rigid body response to both deterministic and stochastic wind, and general elastic body response characteristics.

## Wind Biasing

Wind biasing is concerned with reducing the portion of the bending moment produced by the mean wind. This can be done in several ways since the solution is not unique. One solution that works well commands early inflight vehicle attitude, with the result that the vehicle flies downwind. The wind biasing commands the sign change, thus driving the angle of attack to zero and causing the vehicle to turn into the wind. The peak wind and dynamic pressure occur while the angle of attack is zero, resulting in a

D



low bending moment [5]. An alternate approach flies a low or zero angle of attack for the mean wind until the vehicle leaves the high wind, high dynamic pressure region and then corrects for drift buildup [6].

These techniques can be applied in several ways. If it is assumed that the wind can be measured onboard (roughly), then this information can be stored in the control computer. Through proper filtering, a running mean can be determined for the wind at any flight time based on the past history of the wind. Based on statistics of large scale wind effects, prediction of the wind (running mean) over the next few seconds of flight time can be made and a deterministic wind bias command ( $\psi_c$ ) introduced to cancel it. By updating this information every one-half to one second, a good wind biasing and prediction scheme can be built (Fig. 19).

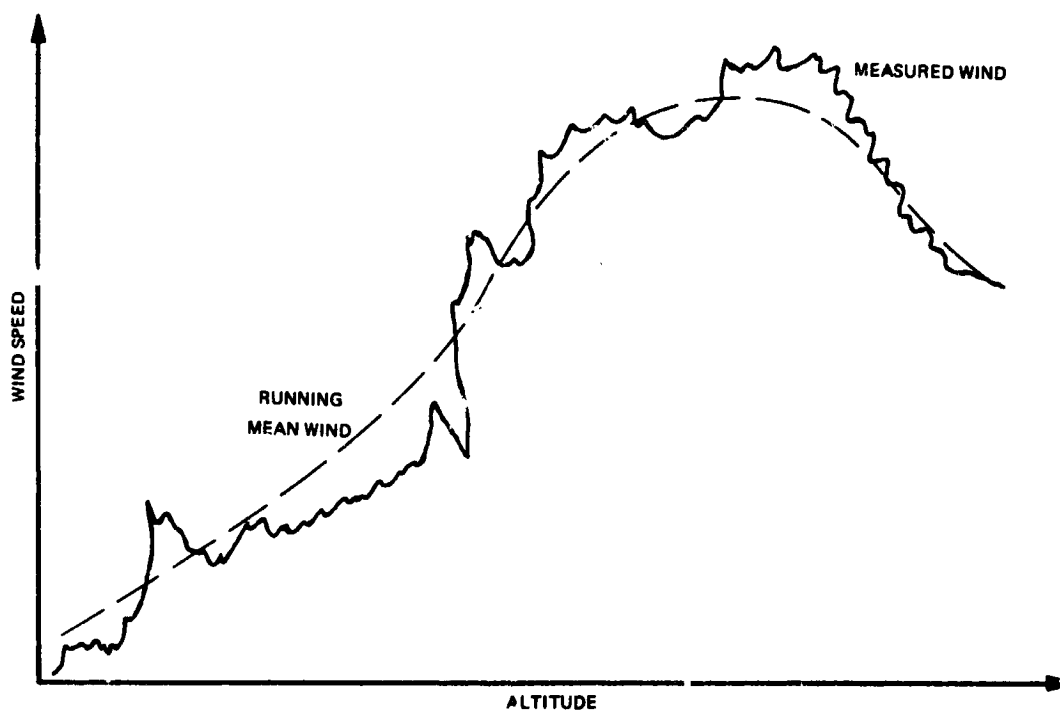


Figure 19. Wind mean prediction and biasing.

Problems associated with inflight wind biasing are numerous. These problems must have solutions before actual use of this technique can be made. These problems are: (1) Biasing is dependent upon the total wind profile shape, particularly during high  $q$  regions. Prediction schemes could conceivably create the wrong trends, thus causing large performance losses.

(2) The prediction scheme must work externally first, since, in general, a space vehicle will fly through the high  $q$  and high winds region within 60 sec, with a corresponding altitude change on the order of 8 km.

(3) Present sensors produce a mixed state estimation. In other words, the sensors not only sense the wind but also the vehicle states, and this could lead to bad prediction values. (4) Storing the wind statistics in order to make good predictions will require large computer capacity. (5) Finally, wind biasing could lead to performance reserve impacts which must be accounted for.

The state-of-the-art wind sensors are a problem which practically forbids this approach. The second best approach premeasures the wind (say one or two hours prior to launch) and establishes a new wind-biased trajectory. This can be accomplished with present high speed computers. This wind-biased control law,  $f(t)$ , is loaded in the flight computer just before flight. There are, of course, the problems of changing and verifying one part of the control computer input just before launch; however, if the software programs are designed properly (in module form), this can be readily done.

A third approach uses the monthly mean wind applicable to launch date, and builds the control logic much earlier. This eliminates last-minute changes, solving the problem of reliability; but biasing to the monthly mean wind does not achieve nearly so much load reduction. Also, elaborate pre-launch wind monitoring procedures, coupled with wind limits, must be used with this approach.

To understand how these schemes reduce loads, and the options available, a simple rigid body yaw plane model is analyzed. Previous launch vehicles, which were symmetrical, had small aerodynamic forces and could easily be described with perturbation equations for load relief control system design. Such treatment was possible since there was only a small influence of the vehicle dynamics on the trajectory and performance and vice versa. The nonsymmetrical Space Shuttle requires much more care in treating the vehicle dynamics. The fact that the large aerodynamic lift forces and moments are not generally zero at the same angle of attack greatly influences not only the control but the trajectory and performance as well. To handle this interaction is a simple matter; it is assumed that the equations can be

divided into two parts: the trim equations about a nominal point mass gravity-turn trajectory, and perturbation dynamic equations about the trajectory trim equations. This approach is generally used, except in the case where the trajectory is shaped in a special way to reduce the angle of attack or the dynamic pressure, or both. In this special case, the trim trajectory is a trajectory which is reshaped about a special trajectory through the high pressure region and then transferred to the basic optimum trajectory for the remainder of the flight. Some payload loss from the optimum is accepted to reduce trim loads.

The coordinate system shown in Figure 5 is used to arrive at the vehicle trim and perturbation equations. The resulting basic planar trajectory equations are:

$$\ddot{\mathbf{X}} = \mathbf{T}_X(\theta, \delta) + \mathbf{L}_X(\alpha, \theta) + \mathbf{D}_X(\alpha, \theta) + \mathbf{G}_X(\chi_c) \quad , \quad (18)$$

$$\ddot{\mathbf{Z}} = \mathbf{T}_Z(\theta, \delta) + \mathbf{L}_Z(\alpha, \theta) + \mathbf{D}_Z(\alpha, \theta) + \mathbf{G}_Z(\chi_c) \quad . \quad (19)$$

Since large aerodynamic and mass trim forces occur, the moment equation must be included:

$$I\ddot{\theta} = I(\ddot{\chi} - \ddot{\chi}_c) = M_N(\delta) + M_R(\delta) + \overline{C_{m_{\alpha=0}}} + \overline{C_{m_{\alpha}}(\alpha)} \quad . \quad (20)$$

The angle of attack is defined as follows:

$$\alpha = \theta - \frac{\dot{Z}}{V_T} + \alpha_W \quad . \quad (21)$$

To divide these equations into trim and perturbation equations, the following trim equations about the trajectory must be satisfied:

$$I\ddot{\theta} = 0 = \overline{C_{m_{\alpha=0}}} + \overline{C_{m_{\alpha}} \alpha_0} + F(Z_{cg} - Z_{\delta}) + \Sigma (X_{cg} - X_{\delta_i}) \delta_{i0} \quad , \quad (22)$$

$$m\ddot{X}_0 = A_x - mg \sin \chi_0 \quad , \quad (23)$$

$$m\ddot{Z} = 0 = mv \dot{\chi}_0 + C_{L_{\alpha=0}} + C_{L_{\alpha}} \alpha_0 + F\delta_0 + mg \cos \chi_0 \quad . \quad (24)$$

These trim conditions use the following values from the point mass trajectory:

$$\chi_0 = \gamma_R \quad \text{the relative flight path,}$$

$$\dot{\chi}_0 = \dot{\gamma}_R \quad \text{the flight path rate,}$$

$$A_X = \quad \text{vehicle acceleration.}$$

The control moment may be derived from various sources such as main engines, surfaces, or reaction jets. Although this paper assumes only main engine control, the extension to surface control is straightforward. Reaction jets would introduce additional nonlinearities which would have to be linearized for use in this type of analysis. The perturbation equations for dynamics become:

$$\ddot{\theta} + C_1 \alpha^* + C_2 \delta^* = 0 \quad , \quad (25)$$

$$\ddot{Z} + K_1 \theta + K_2 \alpha^* + K_3 \delta^* = 0 \quad , \quad (26)$$

$$\alpha^* = \theta - \frac{\dot{Z}}{v} + \frac{V_W}{v} \quad , \quad (27)$$

$$\delta^* = a_0 \theta + a_1 \dot{\theta} + b_0 \alpha^* + f(t) \quad . \quad (28)$$

These equations will be used in later sections also. Since it can be shown that the rigid body acceleration is a direct function of  $\alpha^*$  and  $\delta^*$ , the control equation (28) is valid for accelerometer control also.

If a good indication of load reduction is to be obtained, it is necessary to have the bending moment equation in a tractable form. The bending moment equation was conveniently derived earlier using an aerodynamic distribution defined with zero angle of attack referenced to the vehicle centerline. The distribution in linear form becomes:

$$C_{l_0}'(x) + C_{l_\alpha}'(x)\alpha = C_l'(x) \quad (29)$$

This linearity allows the bending moment to be expressed as:

$$M_B(x) = M_{B_0}(x) + M_\alpha'(x)\alpha(t) + M_\delta'(x)\delta(t) \quad (30)$$

If the  $\alpha$  and  $\delta$  are divided into trim and dynamic perturbation values,

$$\alpha = \alpha_T + \alpha^* \quad (31)$$

$$\delta = \delta_T + \delta^* \quad (32)$$

then the bending moment equation is

$$M_B = \overbrace{M_{B_0}(x) + M_\alpha'(x)\alpha_T + M_\delta'(x)\delta_T}^{\text{Bias and Trim}} + \overbrace{M_\alpha'(x)\alpha^*(t)}^{\text{Perturbation}} + M_\delta'(x)\delta^*(t) \quad (33)$$

As indicated in this split-out, the actual bending moment is a function of the biased aerodynamic forces and the induced trim forces, plus the basic dynamic terms arising from the vehicle dynamics and control characteristics.

To obtain a solution when aerodynamic distributions are unknown, equation (33) is rewritten in the form

$$\frac{M_B(x)}{M_\delta'} = \text{load indicator} = R_{B_0}(x) + R(x)\alpha_T + \delta_T + R(x)\alpha^* + \delta^* \quad (34)$$

By making assumptions for the ratios, this form allows the determination of the effect of the control system, at least in a conceptual way, without knowing the distribution.

Basic trajectories, with vehicle total aerodynamics, allow the computation of the trim terms for the no-wind case. Trade-offs of the trim bending moments at various stations can be achieved, but not without some interaction with the performance capabilities of the vehicles. These trade-offs come about because of the interactions of the various aerodynamic surfaces (at different local angles of attack) and the control that it takes to trim the vehicle. The lift and the moments created by the aerodynamic geometry do not vanish simultaneously (for any one centerline angle of attack), so that a given trajectory must be flown with either an aerodynamic lift force loading the vehicle or a control force for balancing the aerodynamic moment or both for the no-wind case. Control normal force is also produced due to mass offsets from the centroid of the thrust so that a thrust angle with respect to the vehicle centerline is necessary to nullify the engine turning moments produced by the offset. This deflection of the engines is achieved as a bias signal in the trim equation as a counterpart of the  $f(t)$  term in the perturbation equation. The thrust angle offset will, of itself, cause the vehicle to fly at an angle of attack with its attendant aerodynamic loading, and will also alter the thrust angle due to the aerodynamic moment produced by the angle of attack. Trade-offs with station then can be achieved by altering the basic philosophy used to establish the trajectory. A zero aerodynamic moment trajectory calls for the higher aerodynamic ( $q\alpha$ ) loading, but a zero aerodynamic lift trajectory calls for a greater engine loading. Various compromise trajectories can be chosen. With knowledge of the critical stations of the vehicle and the  $M_{\alpha}$  to  $M_{\delta}$  ratios at those stations,

the basic trajectory philosophy can be chosen to reduce the vehicle loadings at the critical stations due to flying a trimmed trajectory. Complete freedom to choose the compromise, however, is not assumed because trajectory drift values will vary with the trajectory philosophy and vehicle payload capabilities will thereby be reduced from their maximums. Additionally, trajectories which fly with an angle of attack far away from the zero moment values may require such large values of gimbals angle for the no-wind trimmed case that, with a limited gimbals capability, insufficient gimbals range is left to handle the effects of the winds encountered. For the total loading picture, the mutual trajectory effects for the no wind or trim loads must be considered, as just discussed, and the trajectory manipulations must be performed to reduce the wind loading effects, which will be discussed next. Assuming that  $V_w$  is the mean wind only, and that no bias terms exist, the object is to determine  $f(t)$  such that the load indicator is a minimum. The most obvious way is to force  $\alpha$  near zero. The near-zero  $\alpha$  has the additional effect of reducing the aerodynamic disturbances acting on the vehicle, thus reducing  $\delta$ . Adopting this procedure assures that

$$\Theta - \frac{\dot{y}}{v} = \frac{-V_W}{v} \quad (35)$$

throughout the flight regime of concern. If this criterion is adopted from lift-off, large angular deviations are introduced since  $\frac{V_W}{v}$  is extremely large in flight because of low vehicle velocity, thus incurring large payload penalties. However, two options are available: (1) keeping  $\alpha$  equal to zero from vehicle lift-off through maximum winds and high dynamic pressure regions, or (2) keeping  $\alpha$  equal to zero only during high loading conditions. By introducing various amounts of lift in the early portions of flight, the zero  $\alpha$  condition in high loading regions can be achieved in any combination of vehicle attitude and lateral drift. This raises the question of which combination is best for the additional wind effects about the mean wind, and which is best to meet trajectory constraints. Obviously, many factors enter the trade-offs: control system logic, terminal trajectory constraints, vehicle characteristics, etc. Figure 20 illustrates these three concepts. Case 1 shows a nonwind-bias case with appropriate wind, angle of attack, etc. Case 2 shows a wind bias that introduces a drift with the wind early in flight and that cancels the wind during the high  $q$  region. No attitude ( $\Theta$ )

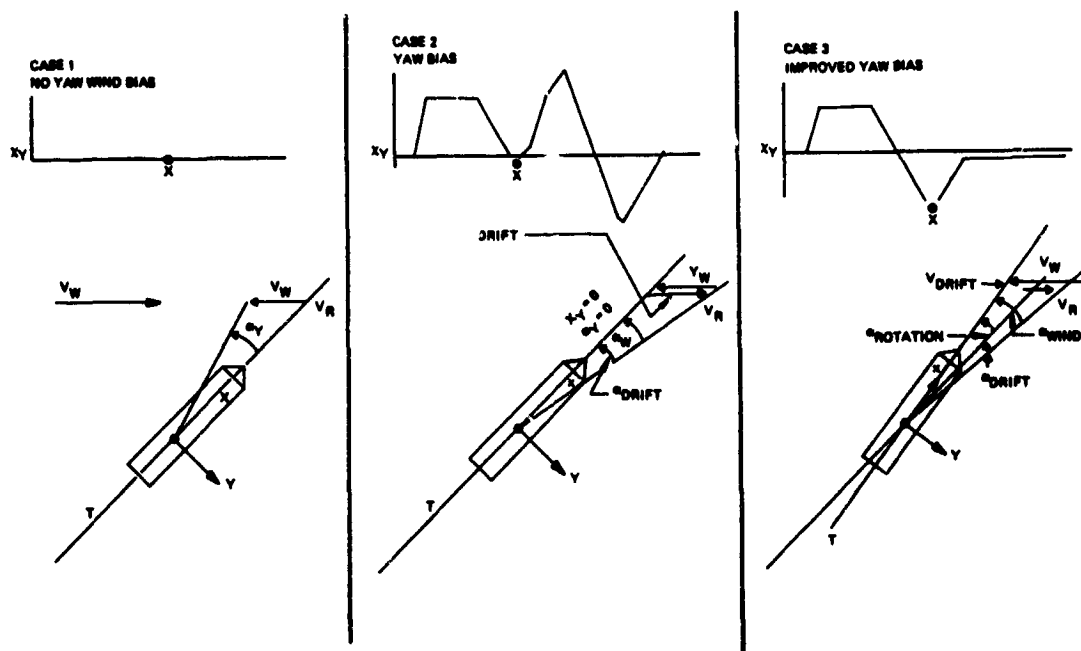


Figure 20. Wind biasing schemes.

is used in this case. This concept results in large terminal drifts and does not reduce the bending moment as much as expected due to biasing because of the overall  $\delta$  to  $\alpha$  induced drift balance. Case 3 splits the desired angle of attack reduction during high  $q$  regions between attitude and drift which results in better terminal conditions, and achieves low bending moments from the mean wind. Figure 21 shows the gain in vehicle wind magnitude capability using the Case 3 type of wind biasing in both pitch and yaw for the Skylab vehicle. Three values are plotted. The solid line is the 95 percent wind rose in terms of wind speed for the month of March showing the predominance of the wind direction from 270 deg. The launch azimuth for this vehicle is 45 deg as shown. The dotted line is the vehicle capability in wind speed without wind biasing. The dot-dash line is the vehicle capability in wind speed using the wind bias. The bias chosen is not optimum since the vehicle capability wind rose could still be shifted to the left to gain more capability.

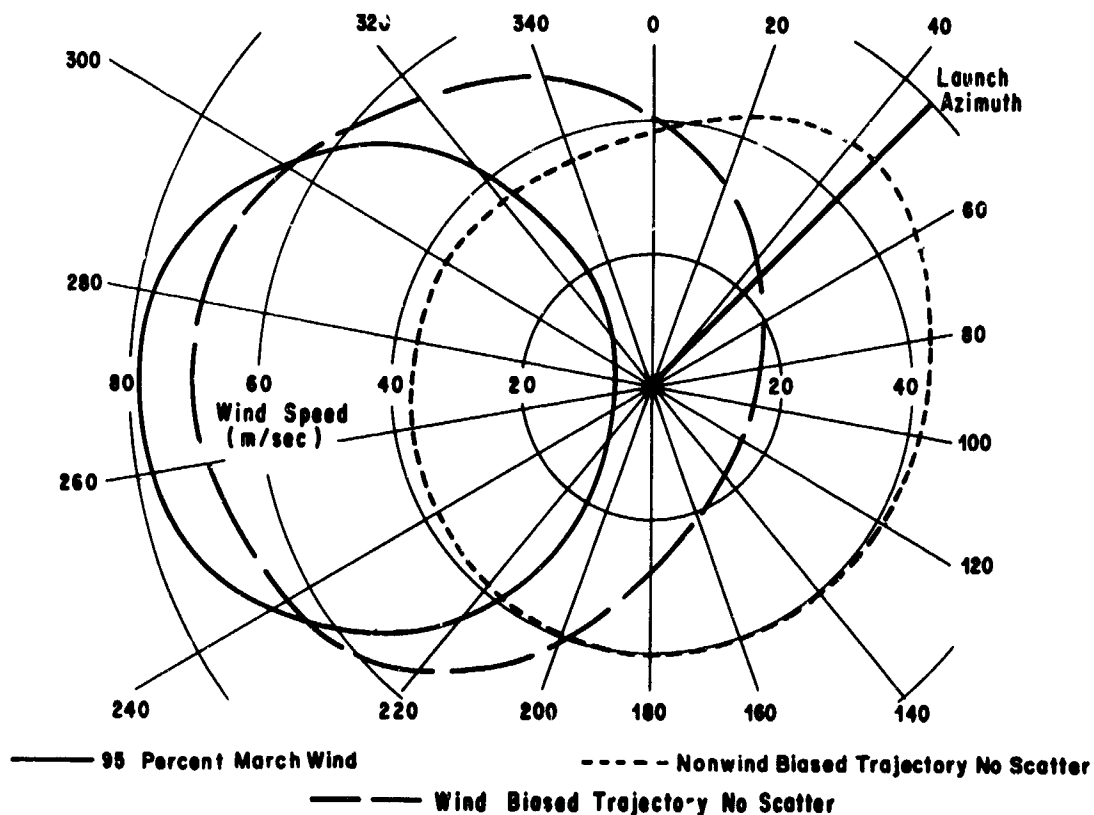


Figure 21. Skylab wind limit - 12 km altitude.



A unique approach is open for the Space Shuttle which may have some merit depending on what conditions design various vehicle elements. This approach is to roll the vehicle in such a way that a minimum load condition occurs at the critical positions. Figures 22, 23, and 24 are the results obtained by rolling the vehicle at various orientations to the wind. As can be seen, the pitch and yaw bending moment can be phased to minimize either plane for winds that have a fairly persistent direction. To accomplish this type of load relief requires the trajectory shaping to be resolved into body-fixed pitch, yaw, and roll commands instead of the conventional pitch command and basically a zero yaw and roll command. This trajectory command resolution does not seem formidable if the approach proves to be desirable. The advantage of this approach for the Space Shuttle appears to be that it can handle early winds without large performance impacts (Figs. 22 through 24). Obviously, for conventional symmetrical vehicles, there is no advantage.

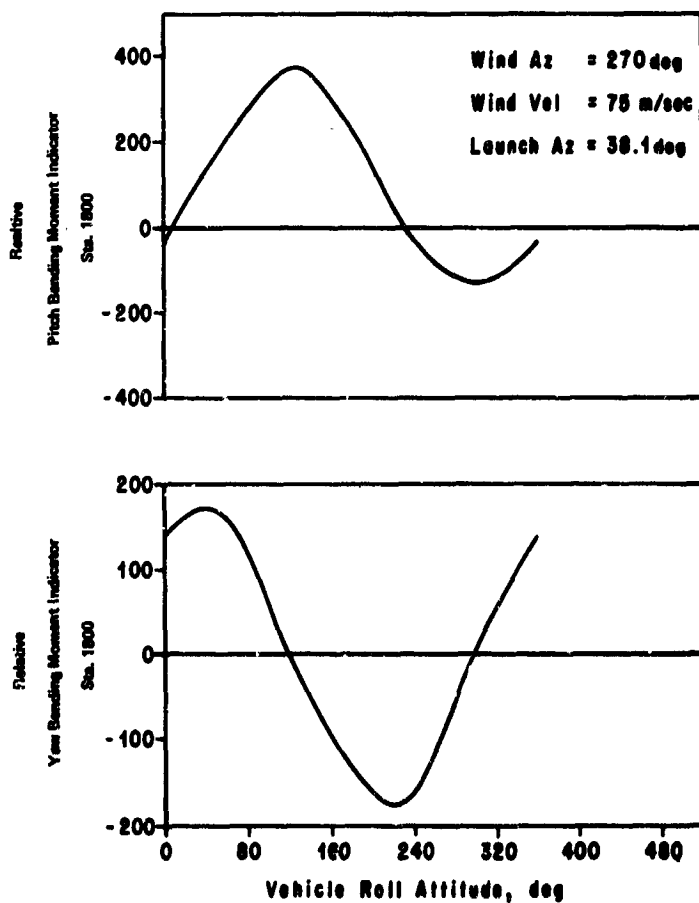


Figure 22. Pitch and yaw bending moment versus vehicle roll attitude.

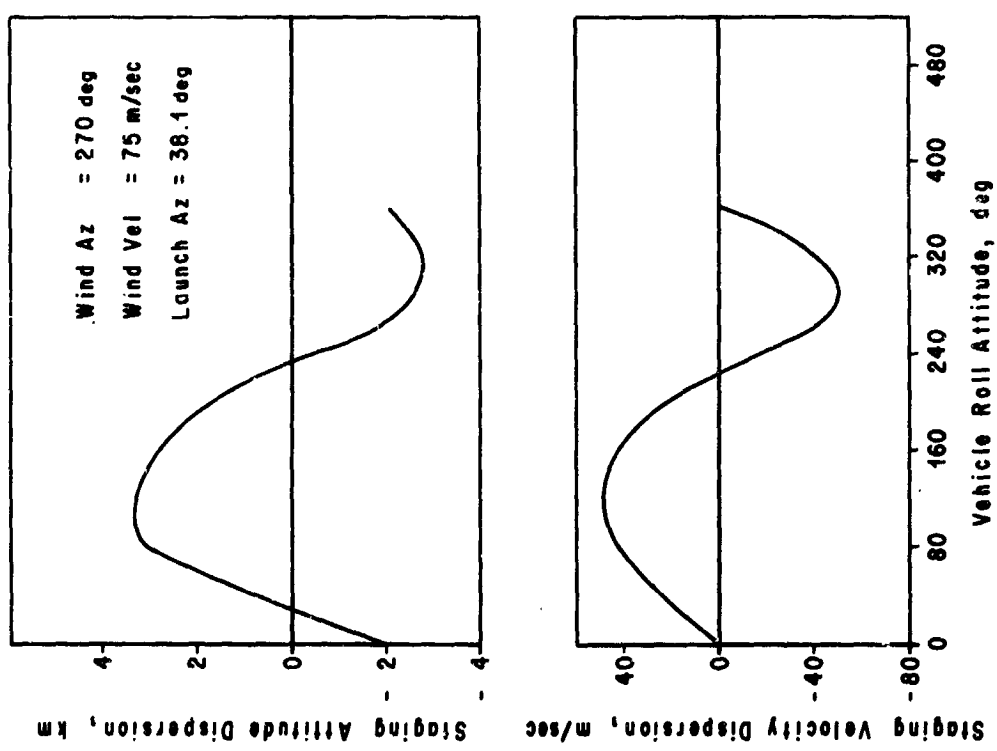


Figure 24. Attitude and velocity dispersions.

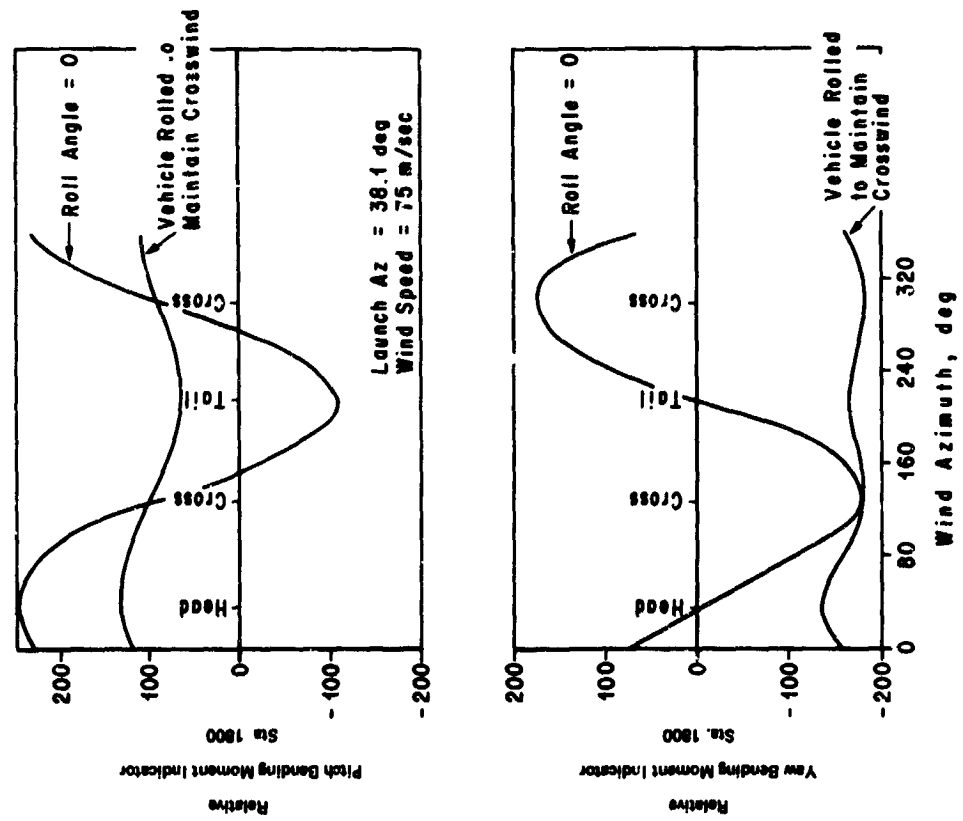


Figure 23. Pitch and yaw bending moment versus wind azimuth.

## IV. LOADS REDUCTION THROUGH ACTIVE CONTROL

### A. Rigid Body Dynamics

The effects of deterministic winds have been discussed in some detail, and some basic logic for implementation was developed by using a very simple attitude control system and a deterministic control function. To understand the effects of the wind variances about the mean, the mean wind and the deterministic control function are eliminated. The representation of the vehicle response as a rigid body gives insight into the interaction of vehicle dynamics and control law so that guidelines for load-relieving control systems can be determined.

Since the control law written with angle-of-attack feedback ( $\alpha$ ) is fairly general, it is representative of several systems. For example, the output of a body-fixed accelerometer can be expressed for rigid-body motion in terms of the source of sensed accelerations, ( $\alpha, \delta$ ), as

$$A_i = \frac{\partial A_i}{\partial \alpha} \alpha + \frac{\partial A_i}{\partial \delta} \delta \quad (36)$$

This produces the same control law with only a modification of gains [7].

Other feedback variables accomplish these same effects, sometimes even more efficiently than attitude, attitude rate, and angle of attack, particularly in combination with accelerometer feedback. For example, translational velocity, position, and integral of the attitude angle can be used in combination with the control law discussed. For the Space Shuttle, which is highly coupled in yaw-roll, crossfeed terms can be included that further reduce loads. These studies are now being made, and will be published in a future report. The trends established here, however, provide the basic insight.

One representative solution to this set of equations is obtained by using frozen coefficients (a conservative assumption, in general) for a representative wind input which is the slow build-up wind (quasi-steady wind profile) or ramp. The characteristic equation of the system, in terms of vehicle parameters, is used to obtain these solutions:

$$S \left\{ S^3 + S^2 \left[ a_1 c_2 - \frac{b_0 K_3}{V} - \frac{K_2}{V} \right] + S \left[ c_2 (a_0 + b_0) + c_1 - \frac{a_1}{V} (c_2 K_2 - c_1 K_3) \right] - \frac{1}{V} \left[ -c_1 K_1 + a_0 (c_2 K_2 - c_1 K_3) - b_0 c_2 K_1 \right] \right\} = 0 \quad (37)$$

A simpler form in terms of the following roots,

$$\begin{aligned} S_1 &= 0 \\ S_2 &= A_1 \\ S_{3,4} &= \sigma \pm i\omega \end{aligned} \quad (38)$$

is

$$S \left\{ S^3 + S^2 (-A_1 - 2\sigma) + S (2A_1\sigma + \sigma^2 + \omega^2) + [-A_1(\sigma^2 + \omega^2)] \right\} = 0 \quad (39)$$

Equating coefficients of powers of S between equations allows the expression of the roots in terms of vehicle parameters and control system gains. A logical choice is to express the control system gains,  $a_0$  and  $a_1$ , and the drift root,  $A_1$ , as functions of control system gain,  $b_0$ , control frequency,  $\omega_c$ , and control damping  $\zeta_c$ ; that is,

$$a_0 = \frac{-\lambda \omega_c^2 B_1 + 2B_3 c_2 \zeta_c \omega_c + \lambda B_3 - c_2 E_2 \omega_c^2}{-2\lambda c_2 \zeta_c \omega_c - \lambda^2 - c_2^2 \omega_c^2} \quad (40)$$

$$a_1 = \frac{c_2 B_3 - 2\lambda B_1 \zeta_c \omega_c + B_2 \lambda - B_1 c_2 \omega_c^2}{-2\lambda c_2 \zeta_c \omega_c - \lambda^2 - c_2^2 \omega_c^2} \quad (41)$$

$$A_1 = \frac{\lambda c_2 B_2 + B_1 \lambda^2 + c_2^2 B_3}{-2\lambda c_2 \zeta_c \omega_c - \lambda^2 - c_2^2 \omega_c^2} \quad (42)$$

where

$$B_1 = 2\zeta_c \omega_c + \frac{K_2 + b_0 K_3}{V} \quad (43)$$

$$B_2 = -c_1 + \omega_c^2 - c_2 b_0 \quad , \quad (44)$$

$$B_3 = -\frac{K_1}{V} (c_1 + b_0 c_2) \quad , \quad (45)$$

$$\lambda = \frac{1}{V} (c_2 K_2 - c_1 K_3) \quad , \quad (46)$$

$$\sigma = -\zeta_c \omega_c \quad , \quad (47)$$

$$\omega_c^2 = \sigma^2 + \omega^2 \quad . \quad (48)$$

Typical plots of the control frequency versus  $A_1$  for the maximum dynamic pressure region of the Saturn V space vehicle are shown in Figure 25. The drift root,  $A_1$ , is stable for zero  $b_0$ , but moves toward instability as  $b_0$  increases. The  $b_0$  value that produces  $A_1$  equal to zero is the well-known drift minimum condition. These results show that the basic influence on the drift root is determined by the angle-of-attack gain,  $b_0$ , and control frequency,  $\omega_c$ .

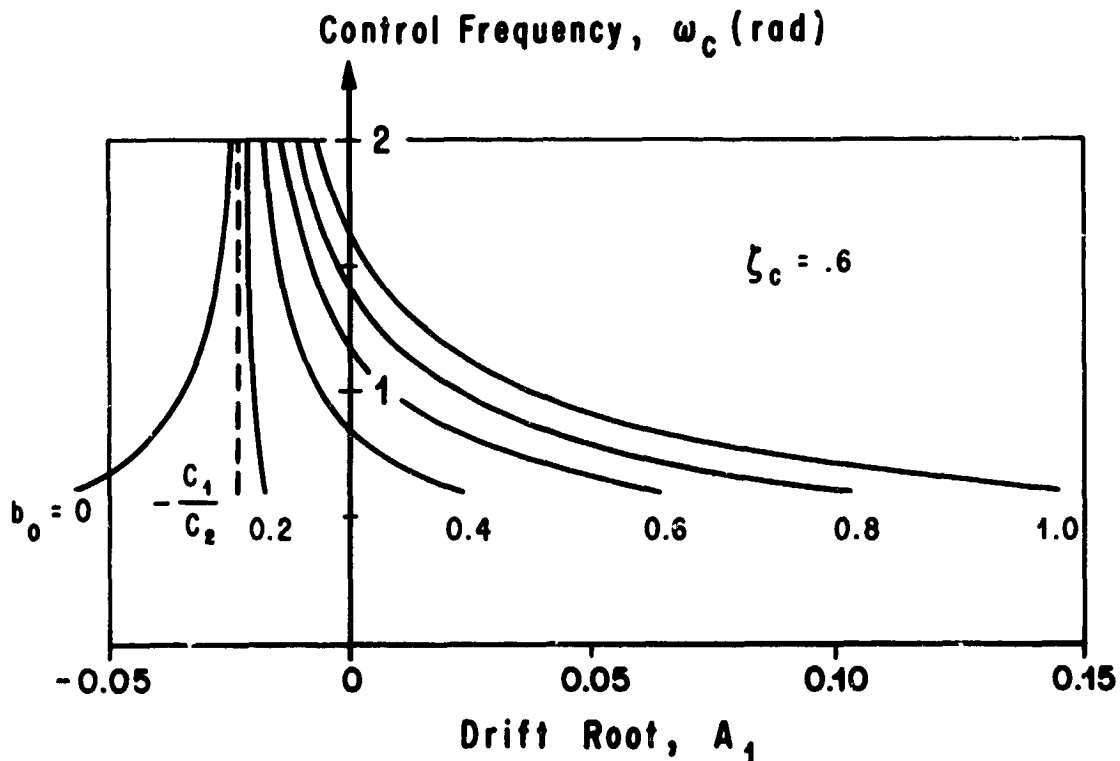


Figure 25. Saturn V control frequency — drift root relationships.

For an aerodynamically stable vehicle, the trends change since the vehicle naturally turns into the wind. Figure 26 shows this change in the vehicle roots and indicates the response change. As indicated by the magnitude and sign of  $A_1$ , large drift occurs. By increasing the frequency  $\omega_c$ , the drift root is reduced in magnitude, thus reducing the drift. The angle-of-attack gain,  $b_0$ , also increases the drift by turning the vehicle into the wind further. This fact indicates that, for angle-of-attack feedback to reduce drift a negative feedback must be used ( $b_0 < 0$ ), or the control frequency increased. Increasing the control frequency is not always possible because of coupling with elastic body modes.

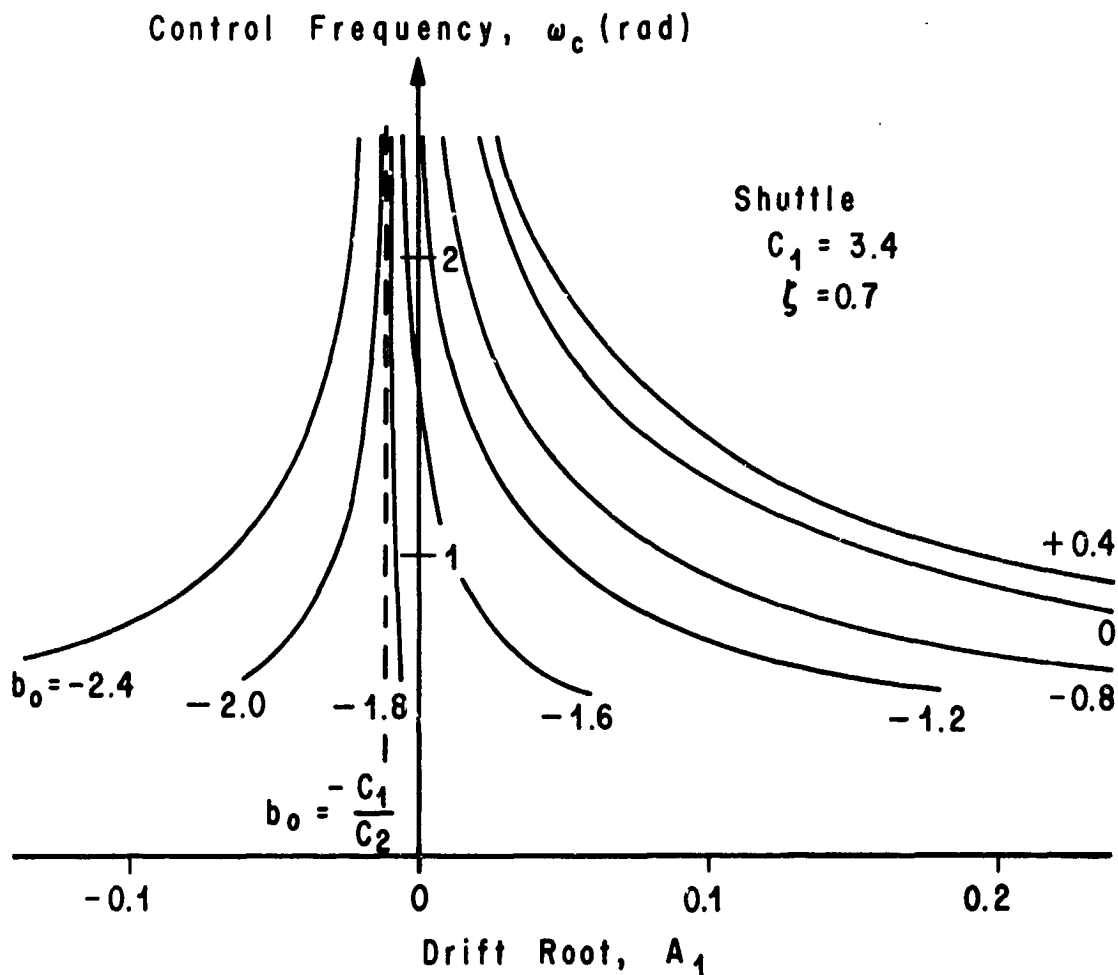


Figure 26. Shuttle control frequency — drift root relationships.

The solution to the set of differential equations can now be formulated in terms of these roots and the system parameters. Only one solution will be analytically formulated: the bending moment response to a ramp wind,  $Kt$ . This solution is sufficient since the time derivative of the ramp solution produces the response to a step, and likewise, the time derivative of the step solution produces the response to an impulse.

The relationships between the roots as a function of control logic that determine the dynamic response are shown on Figure 26. One form of the dynamic response is the bending moment, defined in equation (33). Altering equation (33) for simplicity by removing the trim term yields:

$$M_B(x) = M_{\alpha}^* \alpha + M_{\delta}^* \delta \quad (49)$$

By defining

Note: Stars (\*) have now been dropped for convenience.

$$R(x) = \frac{M_{\alpha}^*}{M_{\delta}^*} \quad (50)$$

$$M_B(x) = M_{\delta}^* [R(x) \alpha + \delta] \quad (51)$$

The actual solution in terms of gains and vehicle parameters is given in Reference [7], and repeated in equations (52) and (53) in generalized form. The bending moment solution for a ramp wind in general form is

$$\begin{aligned} \frac{M_B}{KM_{\delta}^*} &= \overbrace{[\gamma_1 R(x) + \gamma_2] + [\gamma_3 R(x) + \gamma_4] e^{A_1 t}}^{\text{Quasi-steady}} \\ &+ \overbrace{[\gamma_5 R^2(x) + \gamma_6 R(x) + \gamma_7] e^{\gamma t} \sin(\omega t + \psi_1)}^{\text{Dynamic}} \\ &= M_{BQS} + M_{BD} \quad (52) \end{aligned}$$

and the step response is

$$\begin{aligned} \frac{M_B}{KM_{\delta}^*} &= \overbrace{[\theta_1 R(x) + \theta_2] e^{A_1 t}}^{\text{Quasi-steady}} + \overbrace{[\theta_3 R^2(x) + \theta_4 R(x) + \theta_5] e^{\sigma t}}^{\text{Dynamic}} \\ &\quad \overbrace{\sin(\omega t + \psi_2)}^{\text{Dynamic}} = M_{BQS} + M_{BD} \quad (53) \end{aligned}$$

Examining these expressions, we see immediately that the bending moment is composed of three parts for a ramp and only two parts for a step or impulse. The ramp wind has a constant term (a drift root term), which exponentially builds up or decays with the magnitude and sign of the drift root,  $A_1$ , and finally, a dynamic term which is in a damped sinusoidal form determined by the control frequency ( $\omega_c$ ) and control damping ( $\zeta_c$ ). The step and impulse solutions contain only the drift term and the dynamic term. In general, for a ramp wind input, the constant term and the drift root term dominate, while for impulse and sinusoidal inputs, the dynamic term can dominate. The coefficients of these various parts of the solution are also functions of the roots, although not always easily expressible completely in this form. Because of the complexity of the analytical expressions for these coefficients, numerical examples will be presented. In general, a typical wind profile is composed of a mean closely approximating a ramp, superimposed with steps, impulses, and sine functions. The numerical examples are for the step and ramp since they represent the two trends.

A few general statements are in order before looking at specific results. The drift root itself has a unique solution when  $b_0 = \frac{-c_1}{c_2}$ . At this point, regardless of the control frequency or other parameters, the drift root becomes

$$A_1 = \frac{1}{V} \frac{c_2 K_2 - c_1 K_3}{c_2} = \frac{\lambda}{c_2} \quad (54)$$

At this same point [called rotational minimum (R.M.)] the dynamic portion of the solution coefficients is always at a minimum. This is the point at which the angle-of-attack feedback restoring moment cancels the aerodynamic disturbing moment in the rotation equation.

$$\ddot{\Theta} + a_1 c_2 \dot{\Theta} + [c_1 + c_2 (a_0 + b_0)] \Theta = - \frac{\dot{z}}{V} + \alpha_w (c_1 + c_2 b_0) \quad (55)$$

For  $b_0 = \frac{-c_1}{c_2}$  the equation becomes

$$\ddot{\Theta} + a_1 c_2 \dot{\Theta} + a_0 c_2 \Theta = 0 \quad (56)$$

which means that the rotation equation has no aerodynamic forcing term. The drift equation is

$$\ddot{z} + K_1 \Theta + K_2 \alpha + K_3 \delta = 0 \quad (57)$$

Substituting in the rotational minimum condition,

$$b_0 = \frac{-c_1}{c_2} \text{ leads to the equation}$$



$$\ddot{z} - \dot{z}A_1 = -K_3a_1\dot{\Theta} - [K_1 + VA_1 + K_3a_0]\Theta - A_1V_w, \quad (58)$$

which is possible because, at this condition,  $A_1$  is not a function of the control frequency. The second general observation is that a lift minimum load condition (L.M.) produces minimum bending moment coefficients for the exponential portion of the bending moment solution. This occurs when  $a_0$  equals zero. A third general observation is the zero drift of the drift minimum condition (D.M.) which has been discussed previously.

The ironic fact that drift minimum (D.M.), lift minimum (L.M.), and rotational minimum (R.M.) do not occur simultaneously requires trade-offs between these conditions. Elastic body effects, to be discussed in a later section, enter into this trade also.

Three separate launch vehicles were chosen to illustrate how the bending moment is affected through basic control logic. These vehicles cover the class from a highly aerodynamically unstable vehicle to one that is highly aerodynamically stable. The respective characteristics of these three vehicles are seen in Table 1.

TABLE 1. AFFECTED BENDING MOMENT CHARACTERISTICS

Vehicle	$C_1$	$C_2$	$K_1$	$K_2$	$K_3$
1. SIC/Shuttle Orbiter Test Bed	-1.87	1.253	15.00	30.00	15.00
2. SV Apollo	-0.037	1.06	18.58	6.96	15.66
3. One Version of Space Shuttle	+3.371	1.86	20.00	42.79	21.17

Coefficients of the solutions for a ramp and step wind are given versus angle of attack feedback gain,  $b_0$ . The undamped control frequency,  $\omega_c$ , is used as parameter. The control frequency damping is assumed to be 70 percent of critical for all cases.

Figures 27, 28, and 29 are the drift roots,  $A_1$  (not a function of the winds). Looking at the drift root as a function of angle-of-attack gain,  $b_0$ , it is clear that increasing  $b_0$  makes the vehicle more stable in the drift root, while increasing the control frequency  $\omega_c$  makes it more stable (as stated previously). Also, increasing the control frequency decreases the slope of the line of the drift root versus angle-of-attack gain, and thus decreases the effect of angle-of-attack gain,  $b_0$ , on the drift root,  $A_1$ .

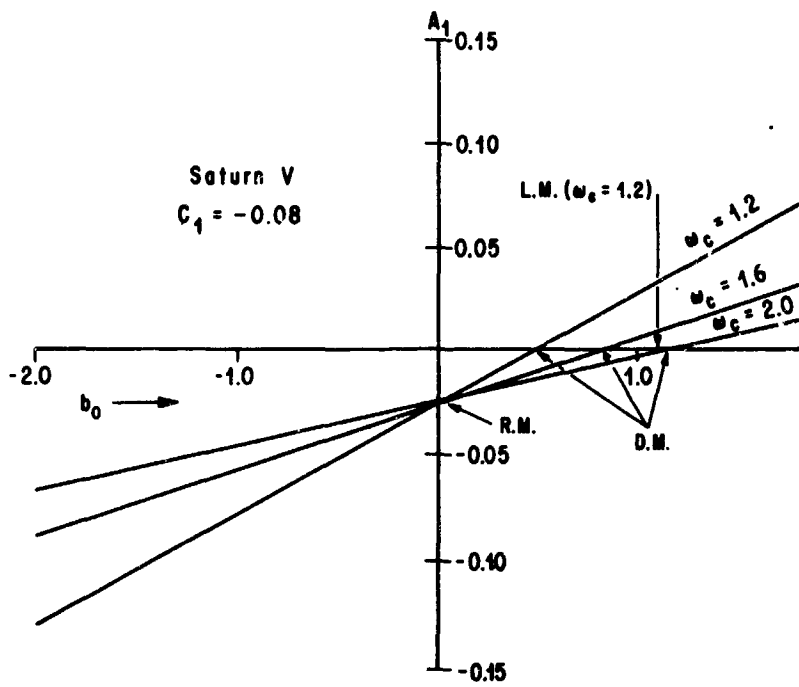


Figure 27. Saturn V drift root versus angle-of-attack gain,  $b_0$ .

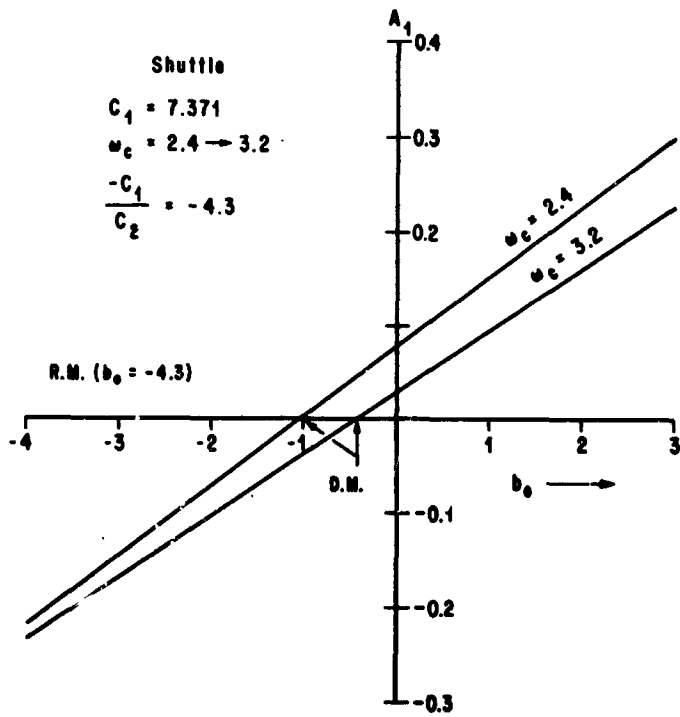


Figure 28. Shuttle drift root versus angle-of-attack gain,  $b_0$ .

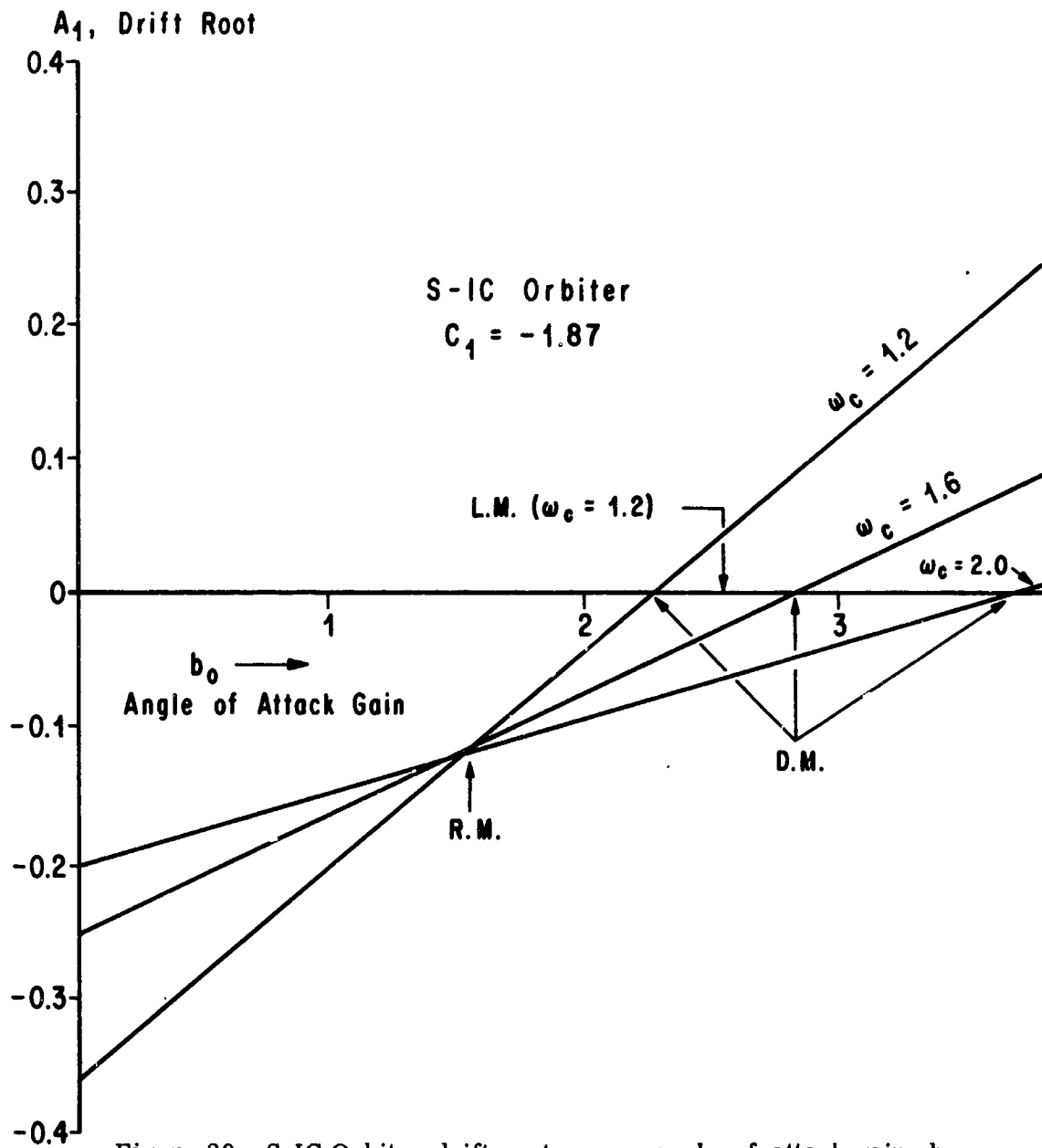


Figure 29. S-IC Orbiter drift root versus angle-of-attack gain,  $b_0$ .

The  $\gamma$  coefficients of the dynamic part of the solution of the bending moment for both the ramp wind and the step wind is decreased in magnitude for increasing control frequency  $\omega_c$ . Also the decay time is faster because a constant 70 percent damping was assumed (Figs. 30 through 36). The effect of angle-of-attack-gain,  $b_0$ , however, depends to a large extent on the vehicle's aerodynamic characteristics. The Saturn V, a slightly unstable vehicle, has increasing magnitudes of the bending moment solution coefficient. On the other hand, the S-IC/Orbiter test bed, also a highly unstable vehicle, has decreasing coefficient magnitudes of the bending moment coefficients until  $b_0$  is approximately 1.6 (rotational minimum), then the magnitude of the coefficients increases for increasing  $b_0$ . For the Space Shuttle, a highly aerodynamically stable vehicle, increasing  $b_0$  increases the magnitude of the coefficients. Choosing  $b_0$  to be negative and increasing its negative value decreases the magnitude of the coefficients. This decreasing trend continues until all control frequencies have zero coefficients. At this same value of  $b_0$ , further increases of  $b_0$  negatively increase the magnitude of the coefficients.

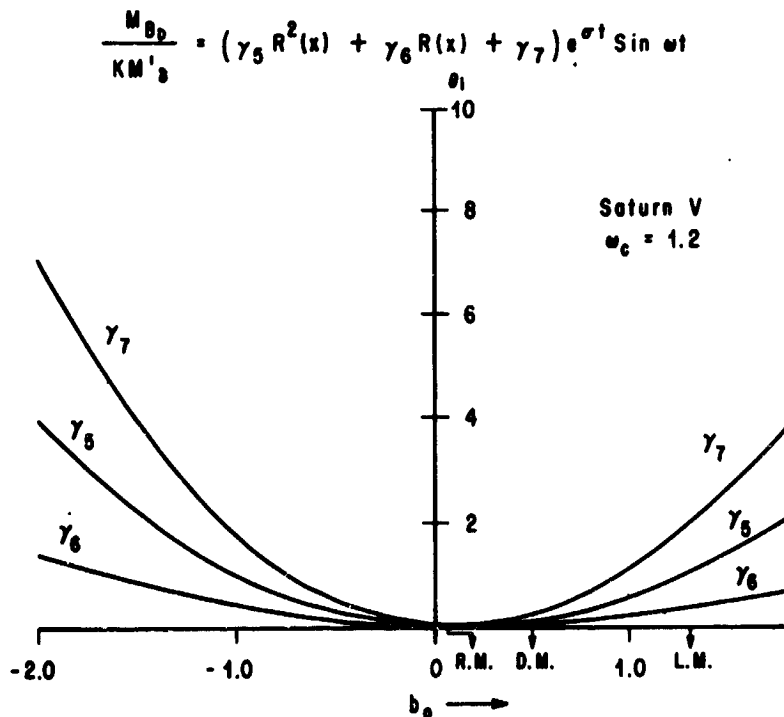


Figure 30. Saturn V dynamic term coefficients — ramp wind.

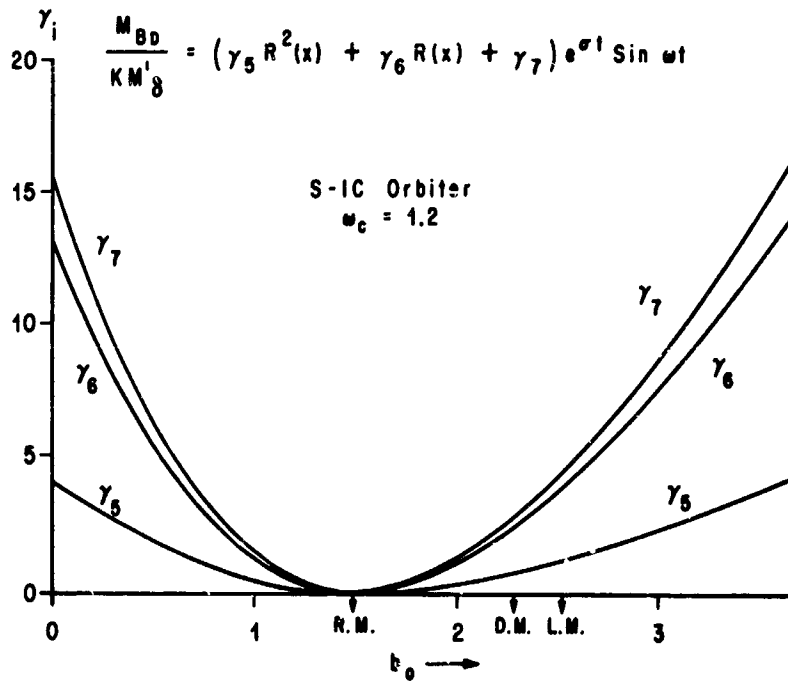


Figure 31. S-IC Orbiter dynamic term coefficients — ramp wind,

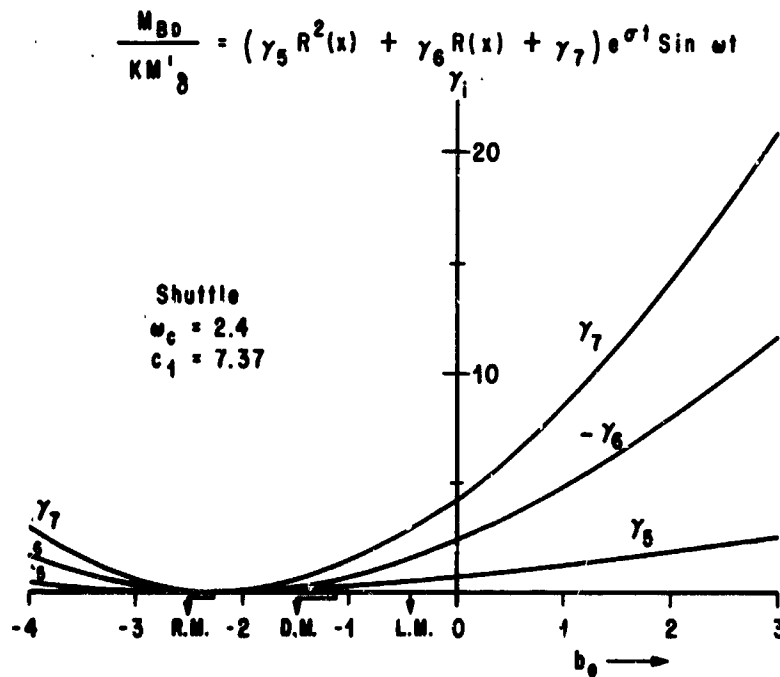


Figure 32. Shuttle dynamic term coefficients — ramp wind.

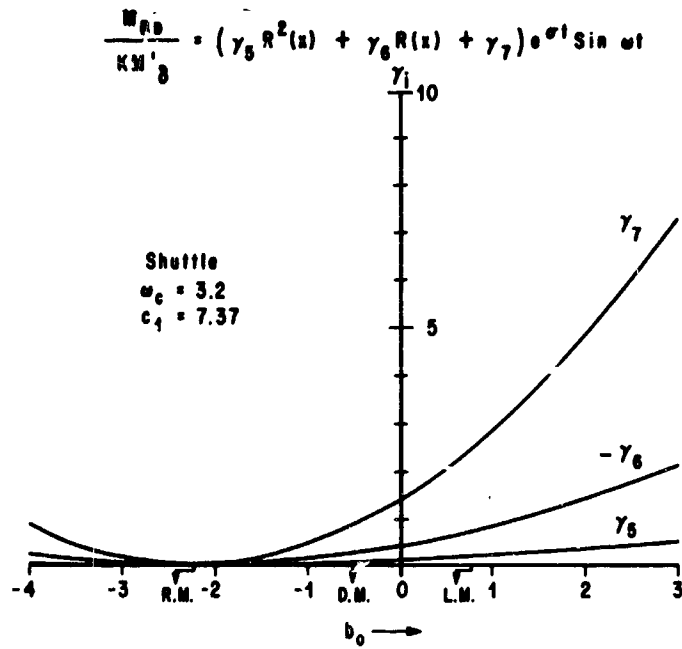


Figure 33. Shuttle dynamic term coefficients — ramp wind.

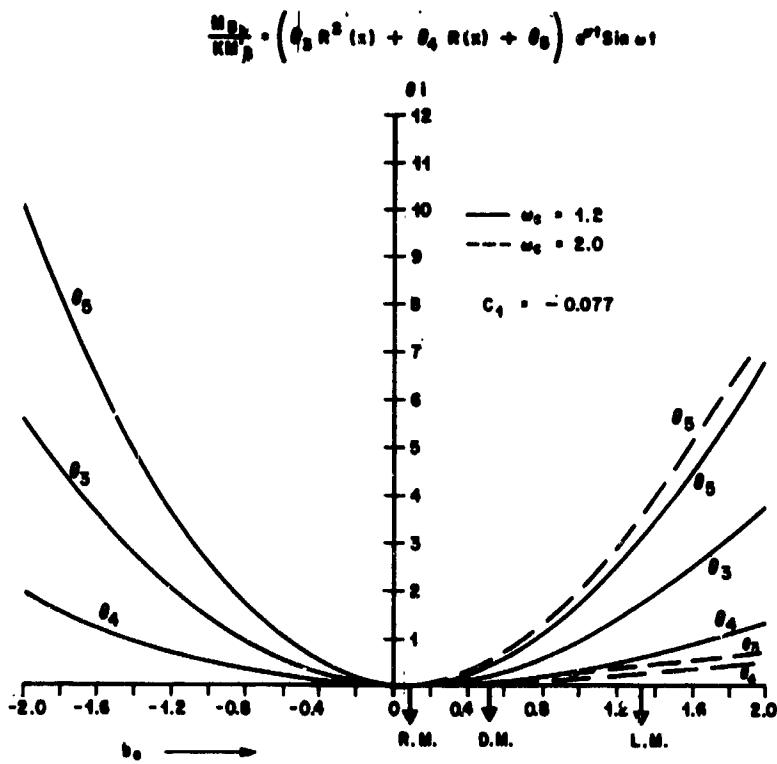


Figure 34. Saturn V — step wind.

$$\frac{M_{BD}}{KM'8} = (\theta_3 R^2(x) + \theta_4 R(x) + \theta_5) e^{\sigma t} \sin \omega t$$

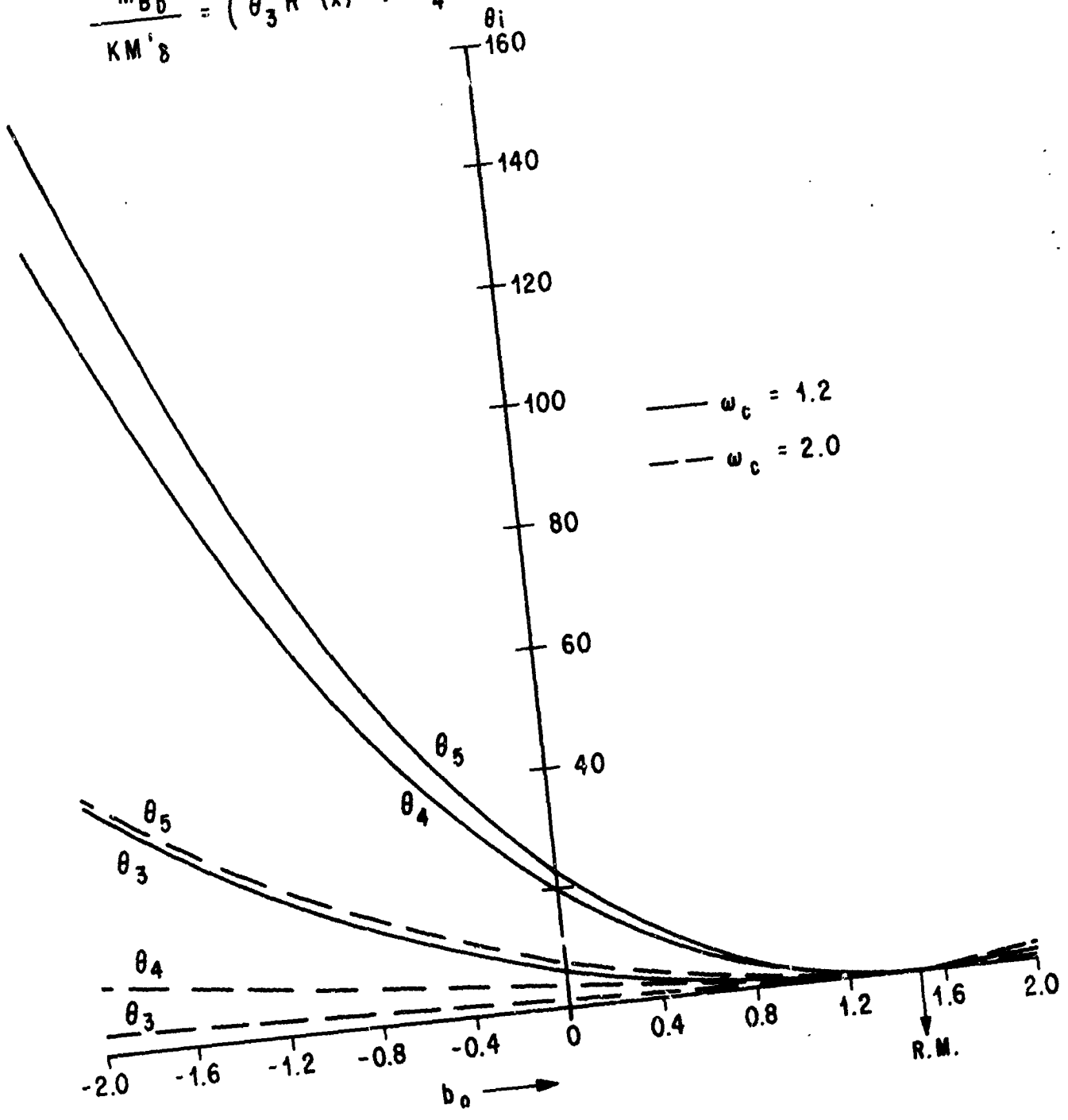


Figure 35. S-IC = Orbiter,  $c_1 = -1.87$  step wind.

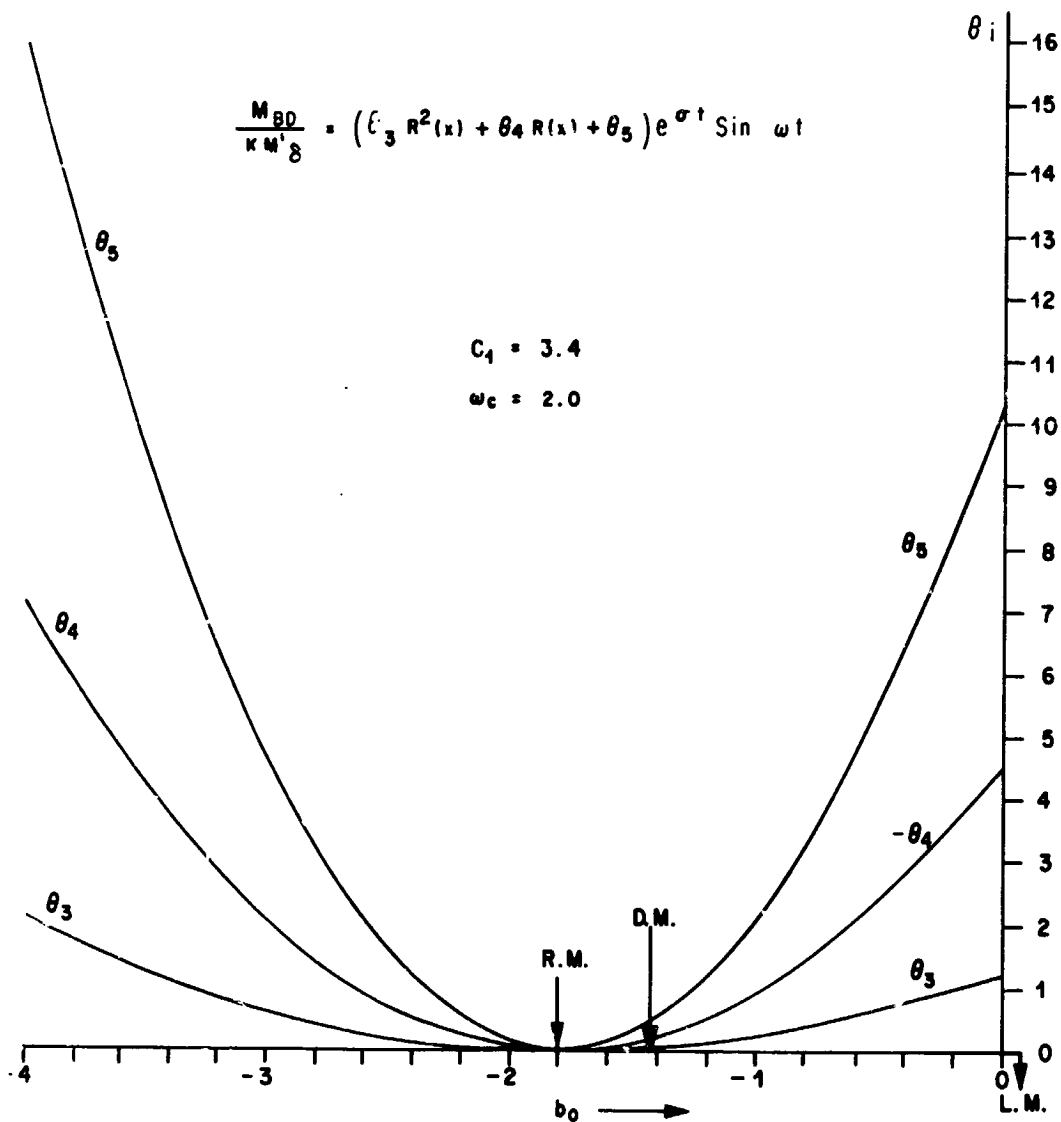


Fig. 36. Shuttle — step wind.

The quasi-steady or drift portion of the solution has some unique characteristics: For the ramp wind (Figs. 37 through 40), two distinct conditions exist; one called drift minimum, where the drift root  $A_1$  equals zero; and the other lift minimum where the bending moment approaches zero. Drift minimum conditions are also good to reduce loads since the terms basically cancel each other for small time spans. The problem with choosing gains near drift minimum occurs if the vehicle must fly at the condition for a long time, thus building up drift and increasing the overall load since the load is a difference of two large numbers with one increasing or decreasing exponentially with the time constant,  $A_1$ .



Saturn V  
 $\omega_c = 1.2$

$$\frac{M_{BQS}}{KM'_\delta} = (\gamma_1 R(x) + \gamma_2) + (\gamma_3 R(x) + \gamma_4) e^{A_1 t}$$

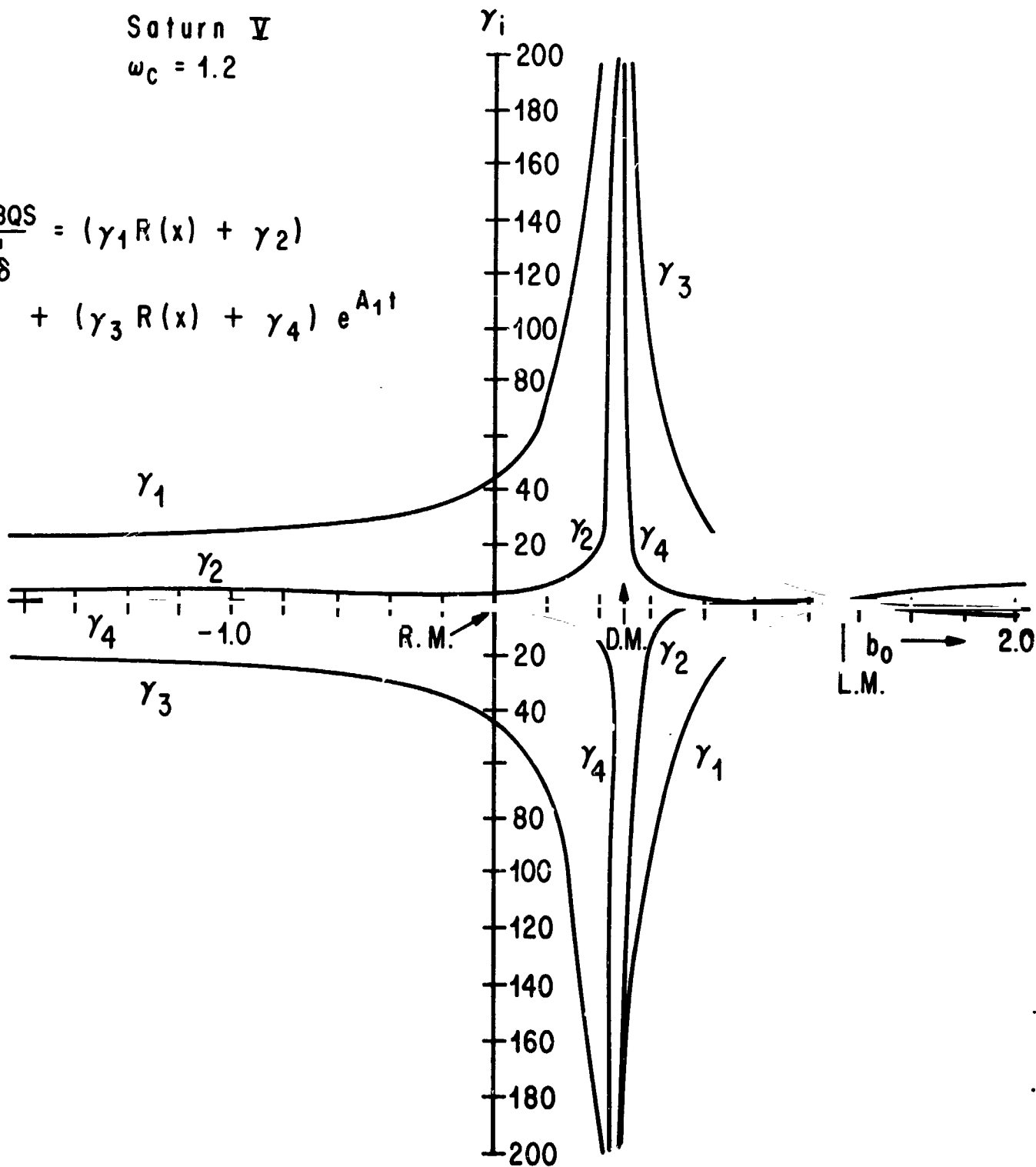


Figure 37. Saturn V quasi-steady term coefficients — ramp wind.

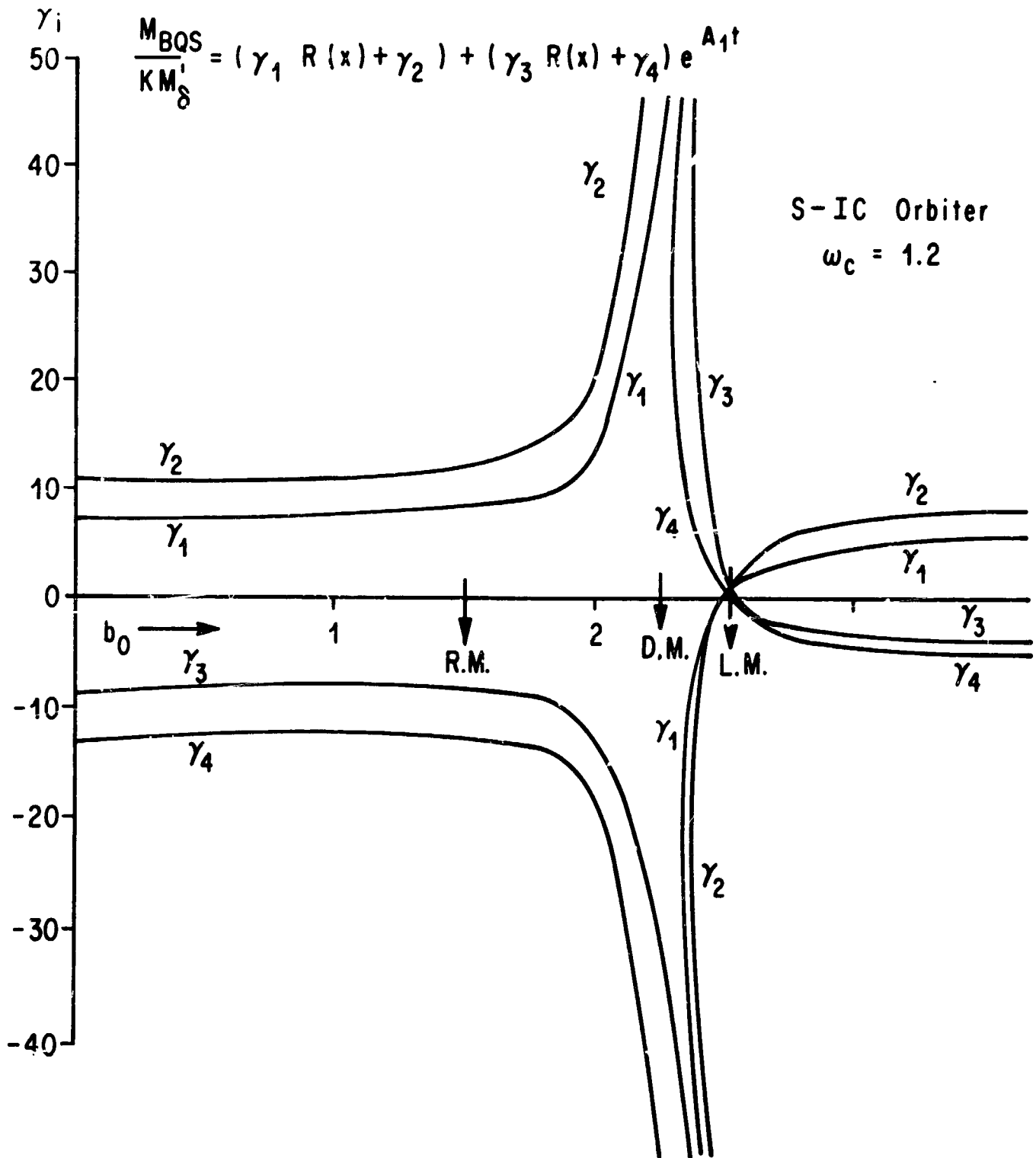


Figure 38. S-IC Orbiter quasi-steady term coefficients — ramp wind.

$$\frac{M_{BQS}}{KM_8} = (\gamma_1 R(x) + \gamma_2) + (\gamma_3 R(x) + \gamma_4) e^{A_1 t}$$

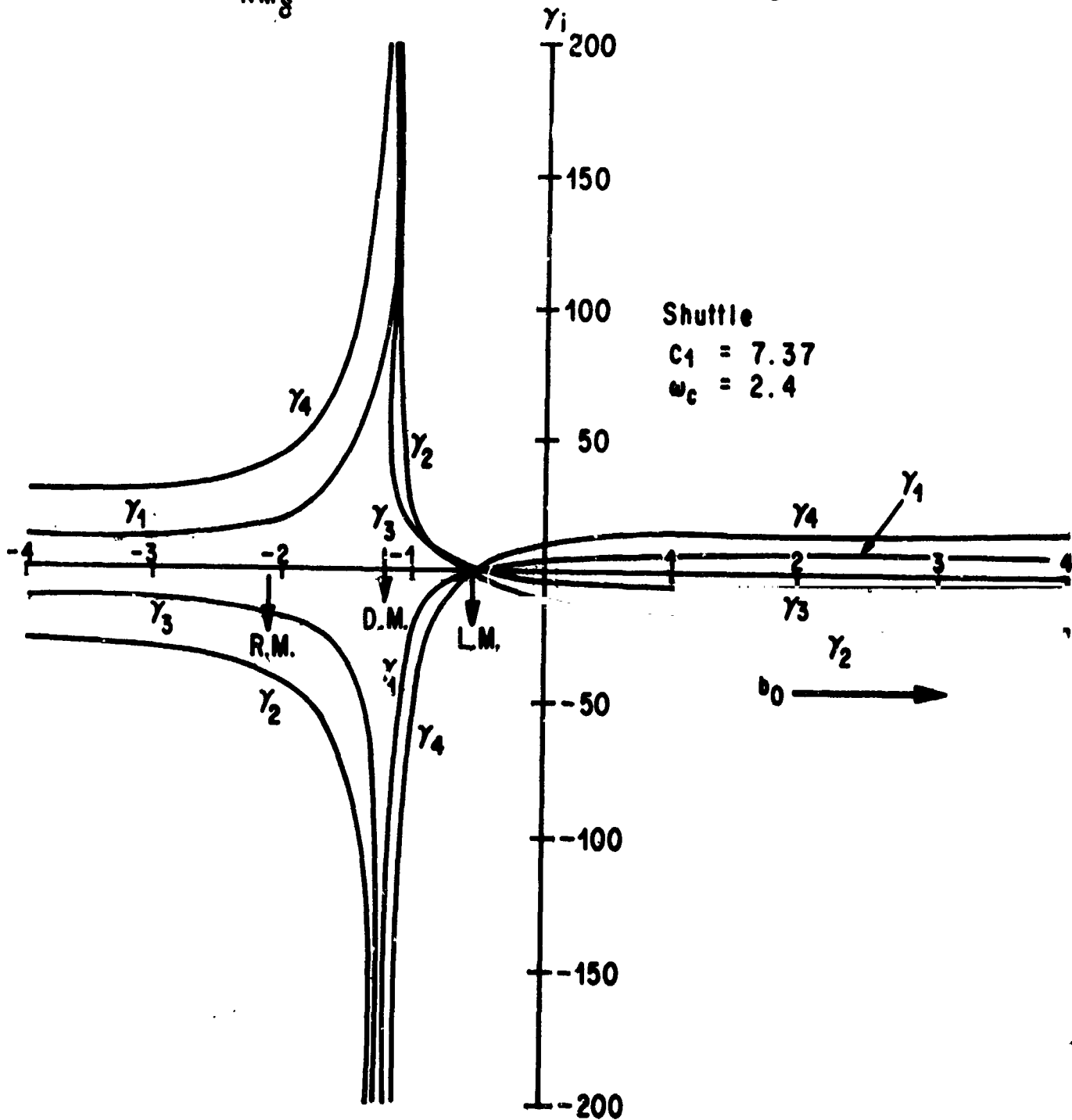


Figure 39. Shuttle quasi-steady term coefficients — ramp wind.

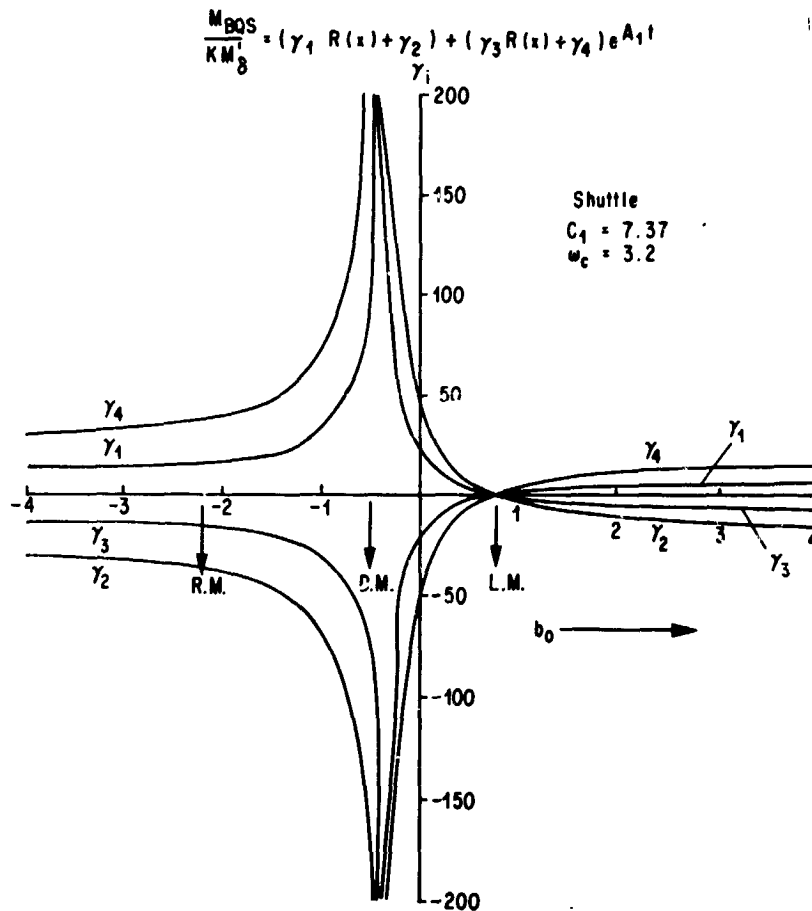


Figure 40. Shuttle quasi-steady term coefficients — ramp wind.

A very interesting difference occurs between an aerodynamically stable and unstable vehicle. In the case of an unstable vehicle, the magnitude of the coefficients (not the difference, which is the actual moment) is large and is increasing until  $b_0$  is increased past the value which produces drift minimum, then the coefficients decrease with further increasing  $b_0$  until lift minimum occurs and then they slightly increase with further  $b_0$  increases. The aerodynamically stable vehicle is in a region of fairly small coefficients which an increase in  $b_0$  does not influence. It does, however, increase  $A_1$ , and thus increases the overall bending moment because of the drift buildup. The drift also results in performance losses. Decreasing  $b_0$ , even to the point of making it negative, moves the vehicle regions towards lift minimum, which occurs before the drift minimum for negatively increasing  $b_0$ . The same lift minimum condition can be reached for  $b_0 = 0$  by increasing the control frequency (Figs. 39 through 40).

In case of a step wind, again the drift portion between an aerodynamically stable and unstable vehicle is different ( Figs. 41 through 43). For unstable vehicles, the coefficients, because of  $\alpha$ , have the same sign as the one from thrust,  $\theta_1$  and  $\theta_2$ , while for the stable vehicle they have opposite signs. This means they partially cancel each other, depending on the magnitude of  $R(x)$  and, in fact, for one particular value of  $R(x)$ , they do cancel. For unstable vehicles, increasing  $b_0$  decreases the magnitude of these coefficients, finally driving them to zero, and then increases them negatively for higher  $b_0$  values. The opposite trend holds for the stable vehicle. Increasing  $b_0$  increases the magnitude, while decreasing  $b_0$  (making it more negative) decreases the coefficients, then finally increases them again.

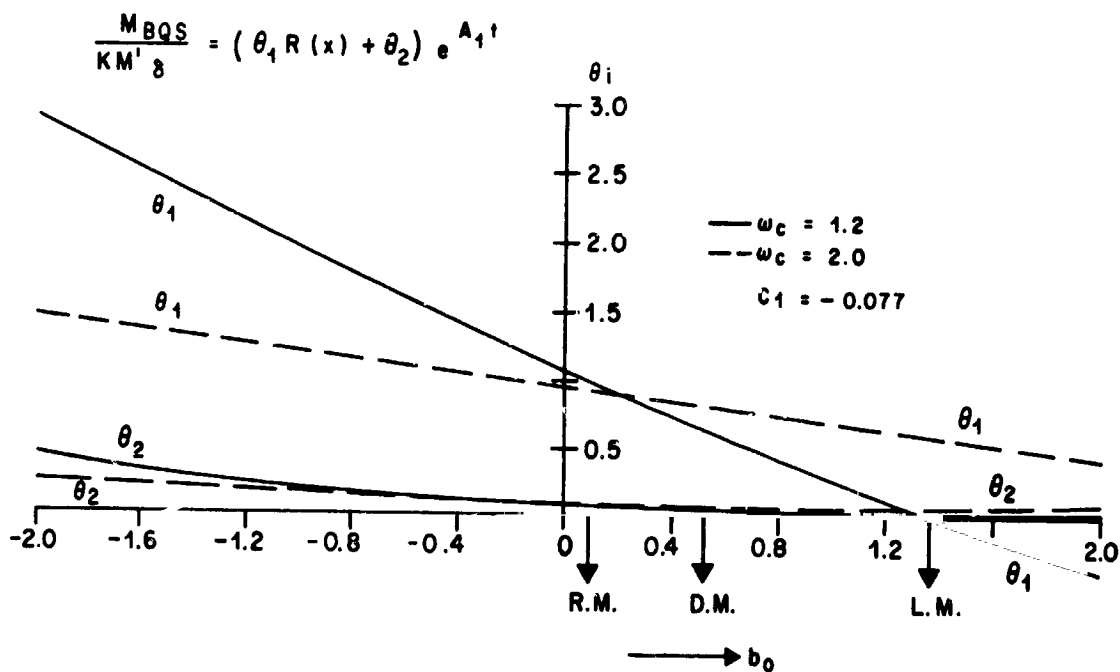


Figure 41. Saturn V — step wind.

The dynamic portion of the solution for the step behaves as it did for the ramp, decreasing with increasing control frequency ( $\omega_c$ ). Minimum values occur where the drift root is the same for all control frequency values (R.M.) with increasing magnitude on each side of this point.

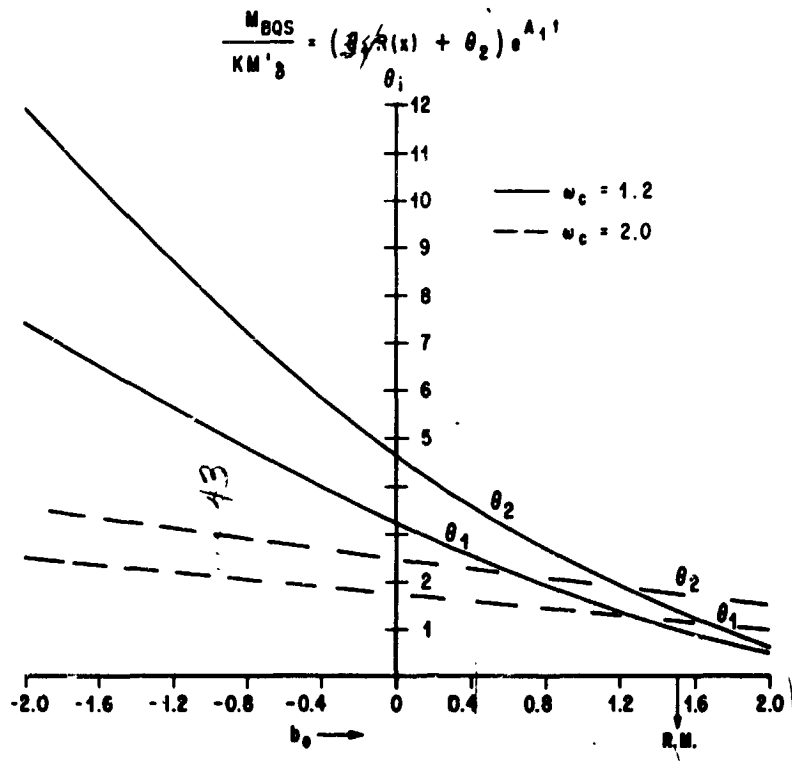


Figure 42. S-IC Orbiter,  $c_1 = -1.87$  step wind.

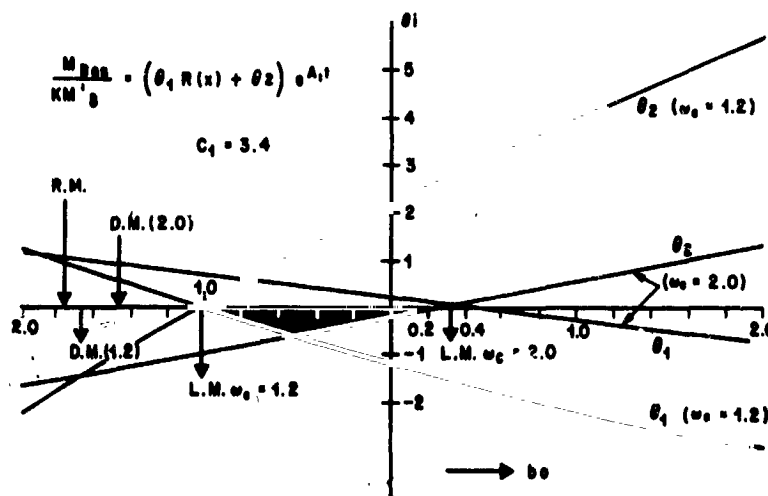


Figure 43. Shuttle - step wind.

The trade-off on load reduction is thus obvious: rotational response versus lateral response, with the best balance being determined by vehicle characteristics, wind characteristics, and mission constraints. To achieve this correct balance requires introducing some angle-of-attack feedback for unstable vehicles, while for stable vehicles the problem is very complex. For the Space Shuttle vehicle presented, the path load (lateral) is very large compared to the rotational (transient) load, which means that one cannot reduce loads by moving gains towards R.M. or D.M. The minimum loads (bending moment) occur when the vehicle is allowed to turn quickly into the wind ( $\alpha_0 = 0$ ) and thus, to accept the induced drift (performance loss), or use additional control feedback logic and variables to try to balance drift and loads. This generalization to all aerodynamically stable vehicles does not hold, however, since different vehicle characteristics could force a different balance (lateral path versus rotational transient loads). Thus, we are able to achieve load reduction by moving towards R.M. or D.M. To illustrate the effect of rotational minimum and drift minimum gains on the time response, a 6-degree-of-freedom simulation was run. The results are shown on Figure 44. There is no rotational motion ( $\theta$ ) for R.M. gains; however, to achieve this requires large gimbal angles and angle of attack; whereas, for lift minimum (L.M.), rotational dynamics are present but at a much reduced angle of attack and gimbal angle response.

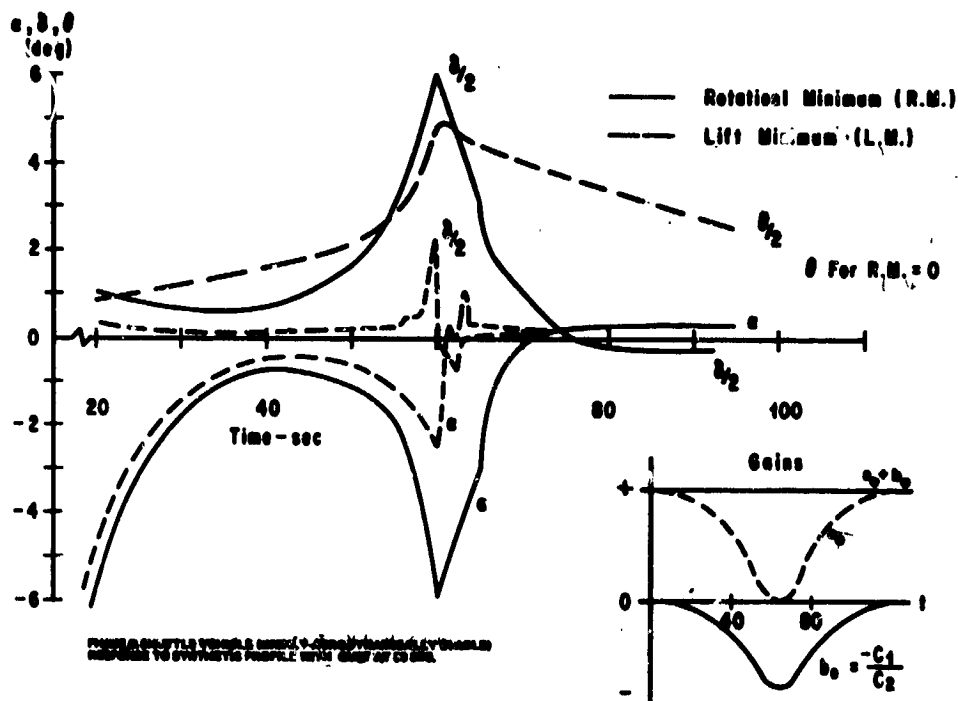


Figure 44. Shuttle dynamic response.

The simplified results show the trade-offs between vehicle drift, rotational dynamics, control authority, and path-following (lateral) loads open to the control engineer. This balance is a function of the vehicle aerodynamic characteristics, mass characteristics, wind characteristics, and control system logic, which must be properly assessed.

## B. Elastic Body (Modal Suppression)

In the discussion thus far, the assumption has been made that vehicle loads are adequately represented by describing the vehicle as a rigid body. Real-life situations quickly reveal that this assumption is not valid and, therefore, the vehicle dynamics must include elastic body oscillations and deflections. Propellant oscillations can, in general, be neglected from the loads standpoint but must be included when vehicle stability is of concern. If propellant oscillations are allowed to become unstable in the closed-loop system, obviously some load influence could result. Since all good designs insure this stability, neglecting sloshing on loads is acceptable. Figure 45 plots the ratio of the bending moment from elastic body dynamics to the total bending moment for various control laws for a Saturn V vehicle.

$$\text{RATIO} = \frac{\sum_{\mu=1}^n M_{\eta_{\mu}}(X, t) \ddot{\eta}_{\mu}(t)}{M_{B_{\text{total}}}} \quad (59)$$

The control system logic used an angle-of-attack feedback with the condition that the control frequency remain constant. It is clear that, on the front end of the vehicle, bending dynamics are very important for bending moment calculations. Also, increasing angle-of-attack feedback, which reduces rigid body loads, actually has the reverse effect on elastic body loads by increasing them. This trend greatly complicates the load relief problem, since the same logic that reduces one basic type of load (rigid body) increases the other (elastic body).

To understand elastic body loads, the assumption will be made (later removed) that one elastic body mode is uncoupled from the other and that the rigid-body angle of attack and engine deflection act as known (timewise) forcing functions to this model. Phasing between engine and aerodynamics is neglected for simplicity. When phasing is neglected, the equation for a bending mode is written as follows:



$$\begin{aligned}
\ddot{\eta}_{\mu}(t) + 2 \zeta_{B\mu} \omega_{B\mu} \dot{\eta}_{\mu}(t) + \omega_{B\mu}^2 \eta(t) &= \frac{F_s Y_E}{M_B} \delta_{\text{elastic}}(t) \\
+ \frac{B_{\mu}}{M_B} \eta_{\mu}(t) + \frac{C_{\mu}}{M_B} \dot{\eta}_{\mu}(t) + \frac{D_{\mu}}{M_B} \alpha_{\text{rigid}}(t) + \\
+ \frac{F_s Y_E}{M_B} \delta_{\text{rigid}}(t) &, \quad (60)
\end{aligned}$$

or

$$\begin{aligned}
\ddot{\eta}_{\mu}(t) + \left( 2\zeta_{B\mu} \omega_{B\mu} - \frac{C_{\mu}}{M_B} \right) \dot{\eta}_{\mu}(t) + \left( \omega_{B\mu}^2 - \frac{B_{\mu}}{M_B} \right) \eta(t) \\
= \frac{F_s Y_E}{M_B} \delta_{\text{elastic}}(t) + \frac{Q(t)}{M_B} \text{ (rigid body forcing function} \\
\text{plus wind gust)} &, \quad (61)
\end{aligned}$$

where

- $\eta_{\mu}(t)$  bending mode generalized coordinate,
- $\omega_{B\mu}$  bending mode natural frequency,
- $M_B$  bending mode generalized mass,
- $\zeta_{B\mu}$  structural damping,
- $B_{\mu}$  local angle of attack aerodynamic term,
- $C_{\mu}$  local angle of attack aerodynamic term,
- $D_{\mu}$  rigid body aerodynamic force term,

$F_s$  vehicle thrust,

$Y_E$  mode deflection at engine.

Assuming that  $\delta_{\text{elastic}}$  results from signals arising from body-fixed accelerometers, rate gyros, and position gyros, the equation becomes

$$\delta_{\text{elastic}} = a_0 \eta_{\mu}(t) Y'(X_g) + a_1 \dot{\eta}_{\mu}(t) Y'(X_R) + a_2 \ddot{\eta}(t) Y(X_A), \quad (2)$$

where  $a_0$  is position signal gain,  $a_1$  rate signal gain,  $a_2$  accelerometer signal gain,  $Y'(X_g)$  the bending mode slope at the position sensor,  $Y'(X_R)$  the bending mode slope at the rate sensor, and  $Y(X_A)$  the bending mode deflection at the acceleration sensor.

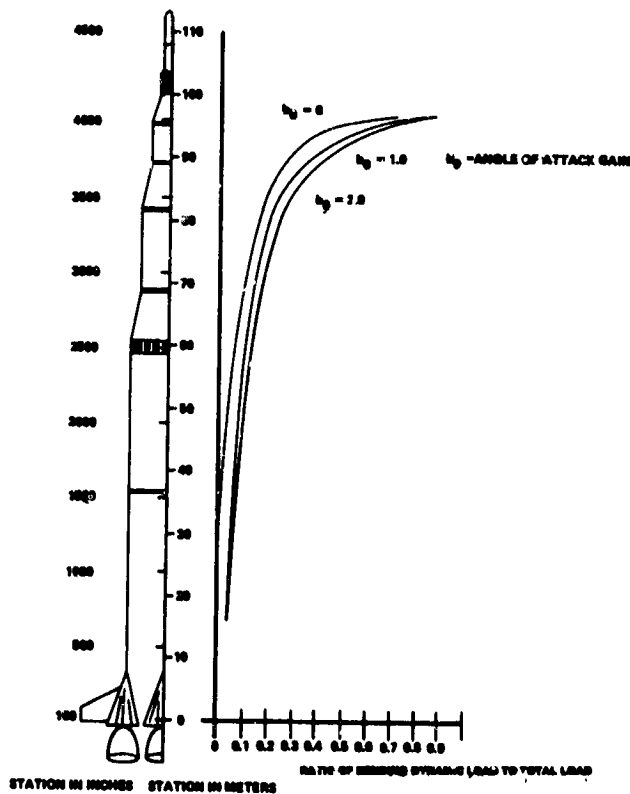


Figure 45. Ratio influence of bending moment due to bending dynamics to total bending moment.

Substituting equation (62) into (61) and simplifying results gives

$$\begin{aligned} \ddot{\eta}_\mu(t) + \frac{\left[ 2\zeta_{B\mu} \omega_{B\mu} M_B - C_\mu - a_1 F_s Y_E Y'(X_R) \right] \dot{\eta}_\mu(t)}{M_B - a_2 F_s Y_E Y(X_A)} \\ + \frac{\left[ \omega_{B\mu}^2 M_B - B_\mu - a_0 F_s Y_E Y'(X_g) \right] \eta_\mu(t)}{M_B - a_2 F_s Y_E Y(X_A)} \\ = \frac{Q(t)}{\left[ M_B - a_2 F_s Y_E Y(X_A) \right]} \end{aligned} \quad (63)$$

It is clear that the above generalizations were made for one sensor; however, the use of more than one sensor does not destroy the use of the analogy, since the total signal is the sum of the voltage coming from each control loop. The effects of multisensors on the roots, and therefore the effects on the response, are not so easily seen because of the possibility of cross-coupling between modes, etc. How the response is altered by these roots is now discussed for the ideal case. The equation becomes

$$\ddot{\eta}_\mu(t) + 2\bar{\alpha} \dot{\eta}_\mu(t) + (\bar{\alpha}^2 + \bar{\beta}^2) \eta_\mu(t) = R^2 Q(t) \quad , \quad (64)$$

where

$$R^2 = \frac{1}{M_B - a_2 F_s Y_E Y(X_A)} \quad , \quad (65)$$

$$\bar{\alpha} = \frac{1}{2} \left[ 2\zeta_{B\mu} \omega_{B\mu} M_B - C_\mu - a_1 F_s Y_E Y'(X_R) \right] R^2 \quad , \quad (66)$$

$$(\bar{\alpha}^2 + \bar{\beta}^2) = \left[ \omega_{B\mu}^2 M_B - B_\mu - a_0 F_s Y_E Y'(X_g) \right] R^2 \quad . \quad (67)$$

$$\bar{\alpha}^2 + \bar{\beta}^2 = \omega_0^2 \quad . \quad (68)$$

The roots to the equation are obviously  $\bar{\alpha} \pm i\bar{\beta}$  defined in equations (66) and (67). Using these roots, the solution to equation (68) gives insight

into load-relieving mechanisms. Typical solutions can be found for constant coefficients and known  $Q(t)$ 's. Assuming that  $Q(t)$  is some known (Laplace) transform, then

$$\eta(s) = \frac{R^2}{\bar{\beta}} \left[ \frac{\bar{\beta}Q(s)}{(s-\bar{\alpha})^2 + \bar{\beta}^2} \right] \text{ for initial conditions equal to zero.} \quad (69)$$

Letting  $Q(t)$  be a ramp input or  $Q(t) = K_3 t$ , then

$$\eta(t) = \frac{R^2 K_3}{\bar{\beta}} \left[ \frac{\bar{\beta} t}{\bar{\alpha}^2 + \bar{\beta}^2} - \frac{2\bar{\alpha}\bar{\beta}}{(\bar{\alpha}^2 + \bar{\beta}^2)} + \frac{1}{\bar{\alpha}^2 + \bar{\beta}^2} \right] e^{-\bar{\alpha}t} \sin(\bar{\beta}t - \psi_4), \quad (70)$$

where

$$\psi_4 = 2 \tan^{-1} \left( \frac{\bar{\beta}}{-\bar{\alpha}} \right), \quad (71)$$

and

$$\tilde{\eta}(t) = \frac{R^2 K_4}{\bar{\beta}} \left[ e^{-\bar{\alpha}t} \sin(\bar{\beta}t) \right]. \quad (72)$$

Finally, if  $Q(t)$  is a sine function

$$Q(t) = K_4 \sin \Omega t, \quad (73)$$

then

$$\eta(t) = R^2 K_4 \frac{\Omega}{\left[ (\bar{\alpha}^2 + \bar{\beta}^2 - \Omega^2) + 4\bar{\alpha}^2 \Omega^2 \right]^{1/2}} \left[ \frac{1}{\Omega} \sin(\Omega t - \psi_6) + \frac{e^{-\bar{\alpha}t}}{\bar{\beta}} \sin(\bar{\beta}t + \psi_7) \right], \quad (74)$$

where

$$\psi_6 = \tan^{-1} \frac{2\bar{\alpha}\Omega}{\bar{\alpha}^2 + \bar{\beta}^2 - \Omega^2} ,$$

$$\psi_7 = \tan^{-1} \frac{2\bar{\alpha}\bar{\beta}}{\bar{\alpha}^2 - \bar{\beta}^2 + \Omega^2} ,$$
(75)

and

$$\dot{\eta}(t) = R^2 K_4 \frac{\Omega}{\left[ (\bar{\alpha}^2 + \bar{\beta}^2 - \Omega^2) + 4\bar{\alpha}^2 \Omega^2 \right]^{1/2}} \left[ -\Omega \sin(\Omega t + \psi_6) + \frac{\bar{\alpha}^2 + \bar{\beta}^2}{\bar{\alpha}} e^{-\bar{\alpha}t} \sin(\bar{\beta}t + \psi_9) \right] ,$$
(76)

where

$$\psi_9 = \psi_7 - \tan^{-1} \frac{2\bar{\alpha}\bar{\beta}}{\bar{\alpha}^2 - \bar{\beta}^2} .$$
(77)

As expected, all cases show a difference between acceleration and displacement to be the  $\omega^2$  factor on the transient part of the solution except for the sinusoidal forcing function which also contains a steady-state term with a factor of  $\Omega^2$  difference. Considering the solution to the ramp, step, or impulse, the magnitude of the constant can be changed by the term  $R^2$  by use of accelerometers. These solutions — ramp, step, and impulse, — can also be altered through each of the sensors as they alter the frequency or damping [ equations (67) and (68) ]. Rate gyros change the damping of the system either positively or negatively depending on the sign of the modal deflection values  $Y_E$  and  $Y^*(X_R)$  and the rate gyro gain,  $a_1$ . Choosing the sensor location or gain such that  $\bar{\alpha}$  increases results in greater damping and lower transient. Choosing an accelerometer location and gain such that  $R$  increases, increases both the damping and the frequency, thus allowing the accelerometer to be used as a modal supressor from both the damping term and the frequency term. Position gyros can be used to alter the frequency by a proper choice of the sensor location or feedback gain,  $a_0$ . The amplitude response (both steady state and transient) in these cases is reduced if the frequency is increased; however, the accelerometer output is proportional to the frequency squared times the transient portion of the solution. Increasing the damping lowers the peak transient response. All three types of input forces are expected during flight since the wind contains some form of each type of input. The response (acceleration or amplitude) can be reduced by increasing the frequency or damping.

A more important type of force from the bending mode standpoint is the sinusoidal input. This represents the turbulence portion of the atmosphere, which can have frequency content in resonance with the bending mode. Also, not only is the transient term important but the steady-state term can be of a larger magnitude in both acceleration and amplitude. Again, increasing the damping decreases the amplitude and thus reduces the transient response. Increasing the frequency may not be feasible, however, since the resonance term contains  $\bar{\beta}^2 + \bar{\alpha}^2$  and  $\Omega^2$ , and the amplitude of the frequency increases as  $\bar{\beta}^2 + \bar{\alpha}^2$  and  $\Omega^2$  approach equal values. In this case the frequency shift must be chosen to detune the system from the forcing frequency. Additionally, for this case, the accelerometer can be used to reduce the overall amplitude through  $R^2$  which multiplies the solution (Fig. 46). Care must be exercised in using this term for reducing amplitude when at the same time it may increase the amplitude through either finer tuning (with forcing function), or decreased damping and frequency. The change in damping and frequency can be obtained by using the various sensors as discussed previously.

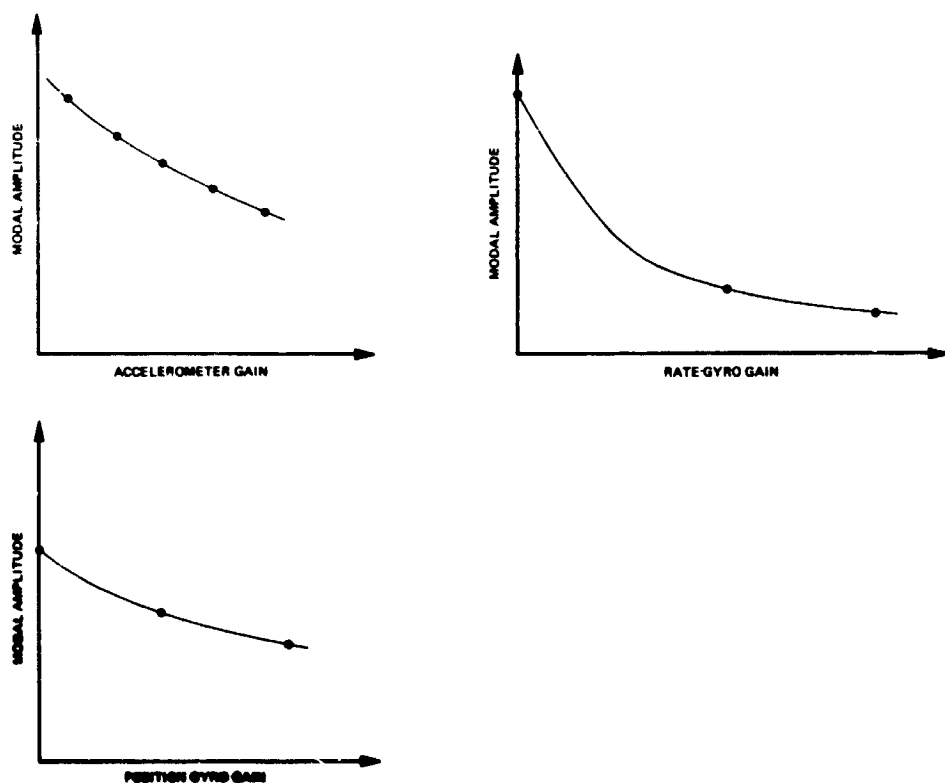


Figure 46. Modal suppression.

The discussion thus far has indicated that accelerometers, rate gyros, or position sensors, can be used for modal suppression. The results point out very clearly that one must have a very accurate description of both the vehicle modal characteristics and the input force (wind) to effectively design a control system for modal suppression using these types of sensors. Also, the coupling of these sensors in the rigid body control (used as input force for mode) is very important and cannot be neglected.

The previous interpretations can be stated in another way. The basic notion here is the freedom offered by a sensor complement in locating closed-loop eigenvalues as a possible source of quality measures. This is motivated by two considerations. First, classical experience with root loci and frequency domain design techniques provides tested insightful relationships between the performance capabilities of a controlled system and the closed-loop pole arrangements permitted by sensors. Such notions as stability, frequencies of oscillation, damping of individual modes of response, and dominance are all apparent from the pole constellation. Second, there is a fundamental connection between pole placement and the concept of controllability.

The previous discussion was based on the assumption that ideal control signals and response exist. Although this is not true, the principles remain the same as long as the gain and phase lag changes that take place in reality are considered. Also, the assumption is made that each mode is completely independent of the other, which is not true. To illustrate this, a two-sensor case will be presented first, then a two-mode case.

If two accelerometers are used instead of one, the denominator in equation (68) becomes

$$\frac{1}{R^2} = M_B - a_{21} F_S Y_E Y(X_{A_1}) - a_{22} F_S Y_E Y(X_{A_2}) \quad (78)$$

This allows a choice of gains and sensor locations that would cancel the accelerometer effect or allow any mixture of effects (gain) between accelerometer locations. The other coefficients in equation (68) could be modified in the same manner by using two or more rate or position gyros. This not only illustrates the complexity of using many sensors but also the flexibility.

Extending the concept to two bending modes, but neglecting certain rigid body coupling, results in the following equations which are derived by assuming only one sensor of each type in the control equation. The control

equation (elastic body feedback portion) is

$$\delta_{\text{elastic}} = a_0 \left[ \eta_1 \dot{Y}_1(X_g) + \eta_2 \dot{Y}_2(X_g) \right] + a_1 \left[ \dot{\eta}_1 \dot{Y}_1(X_R) + \dot{\eta}_2 \dot{Y}_2(X_R) \right] + \epsilon_2 \left[ \ddot{\eta}_1 Y_1(X_A) + \ddot{\eta}_2 Y_2(X_A) \right] \quad (79)$$

The coupled bending dynamics equations given in matrix form, using this control law are as follows:

$$\begin{bmatrix} M_{B1} - \epsilon_2 F_s Y_{E1} Y_1(X_A) & - \epsilon_2 F_s Y_{E1} Y_2(X_A) \\ - \epsilon_2 F_s Y_{E2} Y_1(X_A) & M_{B2} - \epsilon_2 F_s Y_{E2} Y_2(X_A) \end{bmatrix} \begin{Bmatrix} \ddot{\eta}_1 \\ \ddot{\eta}_2 \end{Bmatrix} + \begin{bmatrix} 2k_{B1} M_{B1} - C_{11} - a_1 F_s Y_{E1} Y_1(X_R) & - a_1 F_s Y_{E2} Y_2(X_R) - C_{12} \\ - a_1 F_s Y_{E2} Y_1(X_R) - C_{21} & 2k_{B2} \omega_{B2} M_{B2} - C_{22} - a_1 F_s Y_{E2} Y_2(X_R) \end{bmatrix} \begin{Bmatrix} \dot{\eta}_1 \\ \dot{\eta}_2 \end{Bmatrix} + \begin{bmatrix} M_{B1} \omega_{B1}^2 - B_{11} - a_0 F_s Y_{E1} Y_1(X_g) & - B_{12} - a_0 F_s Y_{E1} Y_2(X_g) \\ - B_{12} - a_0 F_s Y_{E2} Y_1(X_g) & M_{B2} \omega_{B2}^2 - B_{22} - a_0 F_s Y_{E2} Y_2(X_g) \end{bmatrix} \begin{Bmatrix} \eta_1 \\ \eta_2 \end{Bmatrix} = \begin{Bmatrix} Q_1(t) \\ Q_2(t) \end{Bmatrix} \quad (80)$$

The coefficients show that what is done with one sensor for one mode can be offset by the redundant signal from the second mode. If the system is extended to include many sensor gains and force input locations, the trade-offs are apparent but too difficult to formulate. Although the concepts for one mode hold for this more general case of two modes, the design problem is increased many fold because of cross-coupling through the control system. Obviously, the things that help suppress one mode could easily aggravate another. With several modes and sensors, a procedure must be used that provides insight into important characteristics and that gives first cuts at the gain and sensor values and locations.

These system approaches are discussed in section V.



## V. SYSTEM ANALYSIS AND CONCLUSIONS

In the previous section, the basic load-reducing factors were determined based on the assumption that the vehicle's rigid body dynamics, trajectory shaping, and the elastic body dynamics were uncoupled and that the control systems were ideal. These assumptions do not — to a varying degree — hold in the real world. In order to properly analyze the true control system requirements, a complete analysis, including coupling of the vehicle dynamics, structure, trajectory, and "nonideal" control system effects must be conducted. The analysis must also consider a variety of system constraints. The constraints form a development criteria that typically will include: (1) performance margins, (2) attitude restrictions, (3) terminal drift and drift limitations, (4) control system actuator characteristics, (5) vehicle structural capability, (6) control system design goals, and (7) dynamic pressure constraints.

Because the control system must function for a complex, highly-coupled plant with a variety of system constraints, the system design can be a difficult and time-consuming process with many iterations before the final system is developed.

The Phase B Shuttle studies have highlighted this, showing the need for optimizing the total system simultaneously and the lack of a real means for achieving this goal. For example, one Space Shuttle configuration, using conventional trajectory and control concepts, lost 8000 lb of payload capability for a 95 percent headwind. Through a slight configuration change and a combined trajectory-shaping, control-logic blending, this loss was reduced to 1500 lb, a value well within the performance reserves. Examples can also be cited for  $q\alpha$  histories and structural loads. In all cases, the better solutions were obtained through a trial-and-error method. The need is for a combined optimization method that includes all system aspects.

The real value in the application of optimum control theory is its ability to handle large systems with multiple inputs and outputs, and to consider trades on state variable constraints all at once. In addition, the system being analyzed may be linear or nonlinear and constant coefficient or time-varying. However, for large systems, computation usually requires a linearization of the equations about a nominal response. If a quadratic performance index is used with this linearized system, the optimum set of feedback gains may be obtained by solving a matrix Riccati differential equation, the solution being accomplished using a digital computer. It is

interesting to note that without the digital computer the problems that are solvable with optimization theory are limited to a few very simple examples.

Optimization theory and its application are not without their drawbacks and these are areas of current research technology. First, the formulation of an acceptable and meaningful performance index to be minimized is still an area which requires further development. To obtain the closed-form solution discussed above, the performance index to be minimized must be quadratic and positive definite in the state variables and control variables. Some constraints and performance measures do not fit naturally into this quadratic framework, and means are required to be able to consider nonquadratic performance criteria. One such concept uses a nonquadratic performance measure but bounds it by one which is quadratic. In this particular instance, the investigators were able to show that minimizing the quadratic would also minimize the nonquadratic if certain mathematical relationships could be established. Steps in this direction will definitely make the application of optimization methods more attractive.

Secondly, techniques are required to simplify optimal controllers to a practical sensor complement. Optimization by solution of the Riccati equation requires that all vehicle or system states be available for feedback. In large systems this is neither feasible nor possible. Finding ways to move from complete state sensing to a reduced sensor complement for time-varying gains is no easy task. This, of course, assumes that optimality is preserved during the process. No easy solution is available, and some research is being conducted in this area. In most of the cases studied thus far, it does seem advantageous to start with the optimal, full-state, feedback gains and proceed from there to generate the new set of feedback gains for the reduced sensor complement.

Coupled with the problem of using a reduced sensor complement is the question of just what variables are the most important and where should they be sensed on the system being controlled. This is commonly termed the sensor choice and location problem. In principle, this problem is solved by selecting a complement of instruments which exhibits the most desirable cost/performance trade-off, and by locating them optimally along the vehicle. However, as just mentioned, we have no easy methods for evaluation of several sensor complements so that we may evaluate by trial and error which would be the best. A technology effort to determine what are the most important states is certainly a sought-after quantity.

We may summarize by saying that optimization theory is already a valuable tool which can yield useful insight even with its present limitations. If the solutions to these problems can be found, it will surely be the design tool of the future.

The achievement of the best Shuttle design configuration and a consistent load-relief control system is dependent upon five basic factors:

- (1) Analytical or test-derived models of subsystems which are combined into the overall system model. This overall system model must include accurate descriptions of the subsystems, liquid propellant, structural dynamics, control system, aerodynamic forces, and flight mechanics trajectories.
- (2) An accurate description of the environment compatible with the analysis technique. This description is as important as the model because the environment is the major excitation force of both static and dynamic lateral loads.
- (3) Analysis procedures which are efficient lead to understanding, and provide accurate results.
- (4) Performance criteria necessary for performance goal settings both in the design and verification phase, to preclude otherwise ultraconservative designs.
- (5) Active load reduction techniques (mainly control system), which are necessary as a final means of meeting design goals and mission constraints.

The state-of-the-art dynamic-system modeling has reached a high level of sophistication in the last few years. System equations for a 6-degree-of-freedom trajectory, using 3-degree-of-freedom elastic body descriptions, have been formulated. Nonlinear, quasi-steady aerodynamic distributions were incorporated, along with nonideal control systems (filters and lags). Programmed control system gains, time-varying coefficients, and some means of accounting for data tolerances are available.

Even with these advancements, adequate models are still the major problem. A recent publication from NASA Electronics Research Center, entitled "Trends in Control Research and Technology," surveys the most pressing problems facing control engineers. Modeling was listed by a majority of the experts as being one of the major areas of research needing attention today. John B. Lewis, Pennsylvania State University, declares, "There is absolutely no substitute for a thorough knowledge of the system. It is a tedious and time-consuming process requiring much ingenuity to obtain useful system models on which the control design can be based. Good general test procedures are needed so that even complex systems can be satisfactorily described." I. Lefkowitz, Case Western Reserve, says, "We need much more effective means of modeling systems and abstracting from the model the attributes that are relevant to the decision-making and control problem."

Much of the modeling technology needed for vehicle optimization to disturbances is covered in other disciplines, such as structural dynamics. These needs include more accurate elastic-body characteristics that include local effects at sensor locations and mass cross-coupling. Particular emphasis is needed on joints and localized damping. Nonstationary aerodynamics in a practical form for response is a dire need, as well as work in accurately defining the data spreads associated with the characteristics of these subsystems, so that they can be statistically accounted for in the optimization analysis. Finally, an efficient statistical procedure is needed for analyzing these data tolerances along with the final verification analysis.

Four distinct types of wind inputs are available for the appropriate response analysis: (1) discrete, (2) power spectra, (3) nonstationary (stochastic), and (4) individual wind soundings. The accuracy of the vehicle response is obviously directly proportional to the accuracy and understanding of these inputs.

Discrete winds are used mainly as synthetic profiles and 1-cosine gusts. The state-of-the-art profiles are based on many individual soundings and are available for the Eastern Test Range (ETR), Space and Missile Test Center (SAMTEC), White Sands, and Wallops. Wind shear is a conditional shear based on a reference level wind speed. Technology needed for these discrete profiles is a development of joint statistics of the shears and wind speeds.

Power spectra exceedance models for longitudinal, lateral, and vertical gust components are available on a worldwide basis. The power spectra vertical wavelengths of 100m and 2000m are available for the ETR. Additional development is needed to determine the cross spectra from these same data in order to determine more accurate response data.

A nonstationary wind representation is available based on the Rawinsonde profiles (1000m increments) for ETR, and contains interlevel correlations. The major development in this area is the shaping filters and interlevel correlations for the high frequency wind characteristics ( $100 \leq \lambda < 2000\text{m}$ ).

Detailed wind profiles (Jimsphere) based on 25m increments are available for ETR, SAMTEC, White Sands, and Wallops. The present samples are now adequate to duplicate the wind speed and wind shear statistics of the Rawinsonde ensemble. The turbulence portion is also adequate.

Since adequate wind data are available, the major task is the development of a total system model coupled with an efficient adequate optimization tool. To accomplish this goal of optimization requires performance criteria. The following is a list of the present state of the art and technology needed.

## A. Performance Criteria

### 1. State of the Art

- a. Wind - Mean wind plus stochastic (1000m accuracy),
- b. Ideal state and wind sensing,
- c. Constraints on gimbal angle, gimbal rate, and vehicle drift,
- d. Control system optimized to bending moment and terminal conditions.

### 2. Technology Needed

- a. Nonideal state estimation,
- b. 25M stochastic wind model (in process),
- c. Improved optimal procedure for computer efficiency and greater model detail,
- d. Establish validity of present criteria and modify to correct discrepancies,
- e. Develop criteria for bending moment plus other responses, such as crew comfort (acceleration of crew station) (partially done),
- f. Time-varying analogy of frozen point criteria.

Load relief techniques based on optimization of the total system, in this paper, have depended on simple nonadaptive programmed gain techniques and monthly mean wind biasing. With the Shuttle, these concepts need to be extended to adaptive gain scheduling and different wind-biasing schemes.

## B. Load Relief and Modal Suppression

### 1. State of the Art

- a. Programmed gains,
- b. Sensor choice: accelerometers, rate gyros, and position gyros,
- c. Monthly mean wind trajectory biasing (all planes),
- d. Mixed state estimation (modes combined, etc.).

### 2. Technology Needed

- a. Adaptive gain schemes,
- b. Preflight wind biasing schemes,
- c. Inflight wind sensing and wind biasing,
- d. Techniques for designing practical optimal subsystem controller using optimal performance criteria as a goal,
- e. Separate (modes) state estimation,
- f. Technique for minimum interference (coupling) through control system,
- g. Sensor choice and location criteria,
- h. More efficient iteration procedures.

Based on the basic approaches presented in this paper, it is believed that a consolidated, uniform vehicle structural optimization and control system approach is necessary for the Space Shuttle vehicle, and that the compartmentalized approaches of the past will not suffice.

## REFERENCES

1. Papadopoulos, James G.: Wind Penetration Effects on Flight Simulations. AIAA paper no. 67-609, August 14-16, 1967.
2. General Dynamics: A Method for Determining the Response of Space Shuttle to Atmospheric Turbulence. Space Shuttle Turbulence Response, vol. 1, NAS 8-26363, November 1, 1971.
3. Papadopoulos, James G.: Aeroelastic Load Growth Effects on Saturn Configuration. NASA TM X-53634, July 14, 1967.
4. Glanz, William D.: Study for the Indicial Load Effects on Multistage Space Vehicle Systems. NAS 8-11012, Midwest Research Institute, August 20, 1964.
5. Ernsberger, Gale: Wind Biasing Techniques for Use in Obtaining Load Relief. NASA TM X-64604, June 14, 1971.
6. Edinger, et al.: Design of a Load-Relief Control System. NAS8-20155, Honeywell, Inc., May 9, 1966.
7. Ryan, Robert S., and King, Alberta W.: The Influential Aspects of Atmospheric Disturbances on Space Vehicle Design Using Statistical Approaches for Analysis. NASA TN D-4963. January 1969.

APPROVAL

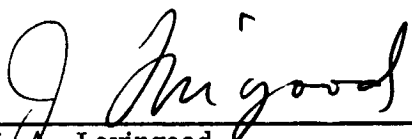
TM X-64684


## FUNDAMENTAL CONCEPTS OF STRUCTURAL LOADING AND LOAD RELIEF TECHNIQUES FOR THE SPACE SHUTTLE

By R. S. Ryan, D. K. Mowery, and S. W. Winder

The information in this report has been reviewed for security classification. Review of any information concerning Department of Defense or Atomic Energy Commission programs has been made by the MSFC Security Classification Officer. This report, in its entirety, has been determined to be unclassified.

This document has also been reviewed and approved for technical accuracy.

  
\_\_\_\_\_  
J. A. Lovingood  
Chief, Dynamics and Control Division

  
\_\_\_\_\_  
E. D. Geissler  
Director, Aero-Astrodynamics Laboratory

☆ U. S. GOVERNMENT PRINTING OFFICE: 1972 - 746-822/4729 REGION NO. 4